# Mechanical perspective on chemotaxis

Chiara Giverso* and Luigi Preziosi
*Department of Mathematical Sciences, Politecnico di Torino, Corso Duca degli Abruzzi 24, 10129 Turin, Italy*

(Received 29 May 2018; revised manuscript received 11 September 2018; published 10 December 2018)

Cell motion in response to external chemical cues (chemotaxis) is a fundamental step in many physiological and pathological phenomena. The ability of cells to move onto two-dimensional flat substrates requires the activation of numerous intracellular mechanical and chemical mechanisms to achieve cell polarization and dynamic assembly and reorganization of the actin network. In this work we aim to bridge the gap between the mathematical models focusing on the mechanics of cell motion and the one describing the final motion of the cell in response to the external chemical field. We thus develop a one-dimensional continuous model representing cell migration, taking into account the mechanical stress inside the cell, the intracellular signaling molecules triggered by external factors, such as an external chemical field, and the actin dynamics during polymerization and depolymerization. The proposed model is solved numerically to simulate cell behavior during biologically relevant conditions and to study different mechanisms of conversion of the external field onto the intracellular chemical messenger, here called the *polymerizing factor*. The model is able to reproduce the transitions from the nonmigrating to the migrating regime, possibly triggered by the external chemotactic gradient, which is amplified by the internal chemical dynamics. More complex migratory behaviors can be described, as well, by including intracellular regulatory pathways of the polymerizing factor. Thus, the proposed model, even though kept as simple as possible, provides an interesting insight onto possible mathematical laws defining cell migratory velocity inside external chemical field gradients.

DOI: 10.1103/PhysRevE.98.062402

## I. INTRODUCTION

### A. Biological background

Cell motility is a complex and dynamic process which is essential for many physiological and pathological conditions, such as wound healing, leukocyte response during immune surveillance, tumor growth, embryogenesis, and morphogenesis [1]. The ability of cells to crawl onto two-dimensional flat substrates requires the spatial and temporal self-organization of the cytoskeleton, a dynamic protein network that extends throughout the cytoplasm, from the nucleus to the plasma membrane, providing mechanical resistance to deformations and allowing cells to migrate.

Cell migration is conventionally described according to a cycle of four active phases, induced by ATP hydrolysis [2–7]: (1) the protrusion driven by polymerization of the branched actin network at the leading edge of the cell (the lamellipodium); (2) the adhesion to the substrate of the protruding part by engagement and disengagement of transmembrane adhesion molecules, mainly integrins; (3) the cytoskeleton contraction due to the activity of myosin motors; and (4) the actin network depolymerization and tail detachment with consequent retraction at the cell rear. Although many aspects of this cycle are shared among different cells, the details can differ greatly, depending on the cell type and on external factors, such as the environmental conditions. In particular, the different steps of the migratory process are observed most distinctly in slow-moving cells, such as fibroblasts, whereas, in fast-moving eukaryotic cells, all the steps are spatially coordinated and are highly synchronized in time, so that the phases follow each other so rapidly that they almost occur simultaneously [7–10]. Furthermore, the inner equilibrium of the system at a subcellular level is actually dynamic, not only when the cell is steadily migrating, but also when it is apparently at rest [11]: the monomeric, or globluar, actin (G-actin) diffuses inside the cytosol and continuously attaches to the barbed ends of the rodlike polymerized filamentous phase (F-actin) while losing monomers at the pointed end (*treadmilling*) [5]. Moreover, the assembled actin filaments are backward transported by the myosin motors (*retrograde flow*) [5,12–15].

To be more precise, recent evidence suggests that different classes of actin filaments exist performing specific functions [16], and at least two populations, the lamellipodial actin and the lamellar actin, are located at the leading edge, contributing to cell motility [17]. These sets of actin filaments are synthesized in response to different stimuli and have different kinetics, and, even though they all require actin-filament assembly into a precise structure (e.g., the helical filaments in eukaryotic cells), they are independently nucleated and disassembled into the common pool of actin monomers [16]. Furthermore direct transitions between the states are extremely rare [16], so that the different actin networks can be considered autonomous.

The initiation of the lamellipodial actin polymerization that leads to lamellipodium protrusion and cell migration requires a polarization of the cell in order to discriminate the leading edge from the trailing edge and implies a loss of symmetry from the stationary nonmoving configuration. Cell

*chiara.giverso@polito.it

 

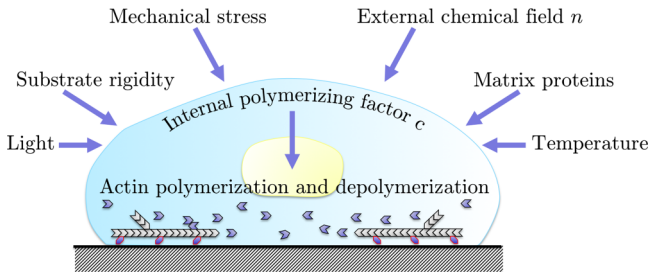


FIG. 1. Various physical, mechanical, and chemical cues can trigger the polarization of the cell and the initiation of the lamellipodial actin polymerization that leads to lamellipodium protrusion and cell migration. Independently from their origin, these external stimuli are converted into internal gradients of signaling molecules, here called the *polymerizing factor*, that in turn guide the cytoskeleton mechanisms performing the motile response.

polarization can be either triggered by various physical and chemical stimuli (e.g., external stresses, substrate rigidity, light, temperature, matrix proteins, or soluble substances), whose asymmetric patterns are detected by the cell and used as an external compass [18,19], or self-regulated (i.e., spontaneous) [20–22], leading to a biased persistent random walk even in the absence of spatial and temporal cues. Independently from its origin, either mechanical or chemical and either external or internal, the stimulus is converted into internal gradients of signaling molecules, here called *polymerizing factors*, that in turn guide the cytoskeleton mechanisms performing the motile response [23] (see Fig. 1). Therefore, in this paper we will focus on cell motion triggered by an asymmetry of a generic polymerizing factor, denoted by $c$, neglecting, in the first instance, the upstream reasons causing this imbalance. In this respect, a discussion of the relationship between intracellular and extracellular signaling and the related consequences can be done *a posteriori*, such as in Sec. III F with particular reference to chemotaxis, which is the directed migration of cells in response to an external chemical field, denoted by $n$.

Specifically, cells can migrate towards the source of soluble chemical agents (chemoattractants) or down the gradient of the chemical in question (chemorepellent). The soluble chemical agent binds to surface receptors [24] and stimulates cells to move in a process that encompasses directional sensing (localization of the source), chemotactic signaling (transmission of the external information to the cytoskeleton by creation of an internal gradient of signaling molecules that act as second messengers to activate downstream molecular pathways), asymmetric cytoskeleton redistribution, activation, and adaptation (through feedback mechanisms in order to dynamically adapt to spatiotemporal changes of external gradients) [19,23–28].

The capability to respond to the external spatial gradient relies on two quantitative parameters: the sensitivity to the relative steepness of the gradient (i.e., the degree of its slope) and the average (midpoint) absolute concentration of a chemoattractant across a cell [19]. Accordingly, cells must possess at least two specialized mechanisms, achieved at the level of second messengers, that enable this type of sensing: *thresholding* (i.e., the ability to subtract the minimum level of signal necessary to activate the downstream response) and *amplification* to allow shallow gradient sensing. These mechanisms are achieved through complex downstream signaling pathways organized into an interdependent redundant network that leads to the activation of many proteins [6].

The major, but not unique, routers of chemotactic signal transmission inside both amoeboid and mesenchymal cells is the PI3-kinase (PI3K) signaling that target molecules of the Ras GTPase superfamily [6,25]. These proteins distribute asymmetrically inside the cell and govern polarization along with directing cell motion. In particular, the PI3-kinase signaling produces the phosphatidylinositol 3,4,5-trisphosphate (PIP3) that acts as an amplifier, sensitizer, and orchestrator of chemotaxis [25]. The Ras GTPase superfamily acts as a common regulator and signal distributor along the front to the back of the cell and contains a large number of molecules, such as Ras, Rac, Rho, and Cdc42. The Ras proteins are attached to the cell membrane and function as a primary hub to set up chemotactic signaling at the membrane. On the other hand, Rac and Cdc42 act at the cell front to establish polarity and initiate lamellipodia expansion via regulated actin nucleation and polymerization [6,25], which is triggered either by catalysers of the polymerization process or more frequently by inhibitors of capping proteins blocking actin polymerization. Finally, Rho GTPases cluster both at the front, where they promote membrane protrusion, as well as at the rear, where they regulate myosin filament assembly and contractility [19,24,25]. We remark that other signaling pathways exist, and they might be either redundant or specific for a particular cell type in order to account for different chemotactic behaviors [19]. Indeed, while the different phases required for cell motility are rather well understood at the cell and macroscopic level, the underlying biochemistry and the mechanics of the whole active continuum system are still under investigation [1,5,29].

### B. Mathematical modeling background

With the purpose of taking a stride towards the quantitative understanding of how cells achieve motion, considering mechanical and chemical cues, the mathematical modeling of cell migration has received an increasing attention over the last years. Due to the various spatial and temporal scales involved in cell migration, numerous modeling approaches have been proposed, addressing different questions. We here briefly discuss only the most relevant literature for the purpose of this paper, and we refer the interested reader to the reviews of the field [9,20,25,30,31]. Specifically, continuous models provide a promising framework for describing cell motility, when the focus is the whole cell or an ensemble of cells, since they are computationally cheaper with respect to discrete models tracking many subcellular constitutive parts. They also allow one to formulate constitutive laws that can be experimentally tested at an observable spatial scale [32]. Continuous models may describe the cell either as a viscous fluid [33–37] or a viscoelastic material [11,38,39] with additional terms to model the active cytoskeleton behavior. Other alternative continuum approaches describe the cell either as a polar gel, in the framework of the theory of liquid crystals, introducing a vector field indicating the local actin filament orientation

[21,40–43], or as a biphasic material, composed by a solid (the actomyosin network) and a liquid (the cytosol) phase [32,44–47], with polymerization and depolymerization represented by mass transfer between the phases. The intrinsically bistable nature (polar versus nonpolar stable states) of the migratory process [20], that makes cells stop (nonpolar symmetric state) or migrate along a specific direction (polar asymmetric state) with various mechanisms corresponding to macroscopically different behaviors and velocities, has been included in these kinds of models in terms of nonlinear constitutive equations for the cellular material [32,45,47], which determine the multiplicity of the stable regimes. Otherwise, the so-called wave-pinning model [37,48] can be used to relate the existence of this bistable cell behavior to the nonlinear exchange between active (membrane-bound) and inactive (cytosolic) forms of proteins (such as the Rho GTPases), that diffuse inside the cell. Notwithstanding, in all the works mentioned above the influence of external stimuli, such a chemoattractant or chemorepellent field, on the migratory process have always been neglected. On the other hand, mathematical models focusing on cell chemotaxis [49,50] generally use empirical laws to link cell motion to the external chemical gradient, without looking at the cell mechanical and subcellular chemical dynamics. Moreover, when the subcellular mechanisms have been addressed, through several excitation-inhibition models explaining the conversion of a shallow gradient of chemoattractant to activation at the front of the cell and internal chemical signaling [51–55], the final cell motion has not been investigated. Only recently, some mathematical and computational efforts have been conducted to account both for cell mechanics along with biochemical cues in the process of cell migration [56–62]. Notable examples are the work conducted by Marée *et al.* [56], that integrates the signaling biochemistry with an actin-based motility model inside a cellular Potts model (CPM) framework, and the pseudopod-centered computational model of Neilson *et al.* [57], in which the outwards normal velocity is proportional to the concentration of a local chemical factor (i.e., the pseudopod activator), and it is counterbalanced by a curvature-based contraction velocity. However, the focus of these preliminary works [56–58] is mainly related to the solution of the dynamics of the signaling molecules and biochemical cues inside a moving cell, without a thorough description of the mechanics guiding the motility process, and the chosen computational framework are not suitable to properly describe stresses and deformations. More recent works [59,59–61] have made a breakthrough on the description of the mechanics of cell motion in response to internal and external chemical cues. Specifically, in the work of Elliott *et al.* [59], the evolution of the cell membrane is guided by a balance of forces that act normal to the surface, whereas in Shi *et al.* [60] a viscoelastic mechanical model has been proposed to simulate cytoskeleton-mediated cellular deformations and movements, in which the local velocity of the cell perimeter is related to the total net stress acting on the cell, including contributions from passive components (i.e., surface tension), protrusive forces (proportional to a signal representing actin polymerization), and elastic stresses (ensuring surface area conservation). However, in these works [59,60] the mechanism of actin polymerization and depolymerization is not included in the model. Finally, in a very recent paper, Moure and Gomez [61] have proposed an interesting phase-field model of cell motion in response to a chemical field, considering cell mechanics. The outstanding two-dimensional and three-dimensional numerical simulations are able to reproduce cell behavior on planar substrates, flat surfaces with obstacles, and fibrous networks. However some biologically observed mechanisms, such as the retrograde flow of actin filaments at the cell boundary, are not included in this framework. Furthermore, this very detailed description of the phenomenon and the complexity of the diffuse-domain approach are unlikely to lead to simple mathematical relations linking the cell velocity to the external field guiding cell directional motion.

### C. Aim of this work

In the present work, we want to make a step towards the mechanical modeling of cell migration taking into account chemomechanical cues. In particular, we believe that, despite the high complexity reached in the numerical simulations of such process [56,57,59–61], the development of a simple one-dimensional model encapsulating mechanical and chemical cues could be of great value in highlighting some peculiarities of cell migration and might allow us to extrapolate possible relations between the cell velocity and the external factor leading to cell motion (e.g., the external chemical field), which can possibly replace well-known equations of cell motions (e.g., the Keller-Segel model for chemotaxis [50]).

In particular, the mathematical model illustrated in this paper is inspired by the work done by Recho *et al.* [35,36] and by Ambrosi *et al.* [37], where a minimal one-dimensional model for an active gel, describing the moving cell, has been presented. Differently from Refs. [35,36] we explicitly define the evolution inside the cell of globular and lamellipodial filamentous actin. Furthermore, unlike previous works [37] that link directly the polymerization and depolymerization only to the cell internal stress, we here introduce the spatiotemporal evolution of the polymerizing factor in response of a given external stimulus, which triggers actin polymerization and depolymerization, also through the inhibition of capping proteins blocking the polymerization of actin filaments.

Without going into details in the whole subcellular network of reactions, whose interactions are still not well understood and seem to be highly cell-specific, in Sec. II we present the theoretical model of cell migration triggered by the spatiotemporal evolution of a generic signaling molecule. The obtained system of equations is then solved numerically, and the results are reported in Sec. III, considering biologically relevant conditions along with the possibility to include *a posteriori* the influence of the external chemical field on the overall process and to obtain bistable cellular behaviors. Finally, the main outcomes of the work and future developments are discussed in Sec. IV.

## II. MATHEMATICAL MODEL

In order to move, a cell needs to polarize and dynamically reorganize, both in space and in time, its actin network and its adhesion to the underlying substrate. As stated in the introductory section, many internal and external factors can lead to cell

polarization and subsequent migration. In particular, in the presence of an external chemical field, the symmetry breaking leading to self-propulsion can be related to the chemoattractant availability: the cell detects the external chemical cue by surface receptors that transmit these signals into the cell, translating the outer signal into a separate, internal one of polymerizing factors, passing through several signaling cascades organized into an interdependent redundant network. In any case, when polarized, the cell loses its circular symmetry, decentering its nucleus and acquiring an elongated shape. The high aspect ratio of a moving cell suggests to represent the moving entity as a one-dimensional strip [39], spanning in the interval $[a(t), b(t)]$ of the $x$ axis, where the location of the boundaries $a(t)$ and $b(t)$ is to be determined. Furthermore, neglecting the curvature of the lamellipodial leading edge and averaging the physical quantities along the vertical and transverse direction [5,36], it is possible to consider the one-dimensional projection of the complex three-dimensional dynamic problem on the direction of locomotion, in order to greatly increase the mathematical tractability of the problem.

At a very general level, the cell can be viewed as a vesicle separated from the exterior by a bilayer lipid membrane, attached from inside to a thin cortex layer maintaining the cell's shape. The interior of the cell is filled with the cytosol, which is treated as a passive medium inside which the nucleus and other organelles are immersed. The active machinery inside the cytosol, responsible of self-propulsion, is given by the cytoskeleton, a continuously renewed network of actin filaments cross-linked by myosin motors, that can exert contractile stresses, and that is mechanically linked to the cell exterior through the dynamic expression of adhesion proteins [2]. These sites of adhesion act as molecular clutches that provide grip to the substrate for the lamellipodium to protrude forward during motility. This interaction between the cell and the substratum can be assumed to be passive [36,37], and the generated shear stress can be represented, in this minimal setting, as a drag viscous force proportional to the lamellipodial actin-averaged velocity. Following [36,37], the one-dimensional continuum layer representing the cell is in frictional contact with the background, assumed rigid, and the balance of linear momentum, neglecting inertia, reduces to

$$\frac{\partial \sigma}{\partial x} = \beta v, \tag{1}$$

where $v(x,t)$ is the vertically averaged horizontal velocity of the lamellipodial actin network (measured with respect to the rigid substrate) and $\beta$ is a frictional parameter representing the dynamical adhesion between the cell and the substrate. In principle, the frictional parameter should be related to the engagement and disengagement of transmembrane receptors mediating adhesion, whose dynamics could depend on both intracellular and extracellular mechanical and chemical cues (e.g., the chemoattractant concentration, the rigidity of the substrate, or the intracellular signaling molecule). However, in a first approximation it is reasonable to take it constant. Then we consider that the cell behaves as a one-dimensional viscous gel with a spatially homogeneous prestress, representing active contraction generated at the microscale by molecular motors [12,39,41,63], so that, after vertical and transverse integration, the stress $\sigma(x,t)$ inside the cell reads

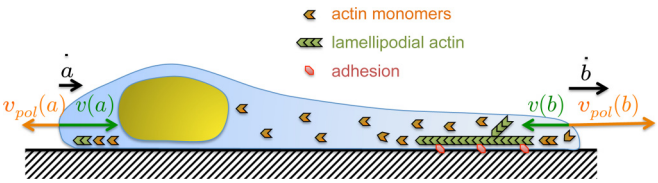


FIG. 2. Schematic representaion of lamellipodial actin polymerization and depolymerization and retrograde flow inside a moving cell.

$$\sigma = \chi + \mu \frac{\partial v}{\partial x}, \tag{2}$$

where $\chi$ is the contractile active stress and $\mu$ is the shear viscosity of the actin meshwork, seen as a continuum gel, moving with the same velocity $v$ as the lamellipodial actin network. We remark that in principle, $\chi$ could depend on some internal molecular signaling and on the distribution of myosin motors, but in a first approximation it could be considered constant, assuming that the chemicals do not significantly influence the active stress generation and that the myosin motors are uniformly distributed [37]. Furthermore, it is reasonable to neglect the bulk elastic stresses of the cell since it relaxes over a timescale of 1–10 s [11,35,64] which is much shorter than the characteristic timescale of motility experiments (some minutes up to hours). Thus, while the actual rheology of the cell cytoskeleton is much more complex [65], such a simple model is sufficient to point out some basic mechanisms of cell locomotion, and therefore it is well accepted [36,37,39].

Combining Eqs. (1) and (2), we obtain

$$\frac{\mu}{\beta}\frac{\partial^2 \sigma}{\partial x^2} - \sigma + \chi = 0, \tag{3}$$

which, coupled with proper dynamic boundary conditions (BCs), gives the evolution of the stress inside the cell.

In particular, accounting for the tension of the cell membrane [37], we can set

$$\sigma(a(t)) = -k[L(t) - L_0],\ \sigma(b(t)) = -k[L(t) - L_0], \tag{4}$$

where $k$ is the membrane elastic modulus, $L(t) = b(t) - a(t)$ is the length of the cell, and $L_0$ is the length of the cell for which no tension is exerted at the cell ends. Then the cell motion problem is totally defined by prescribing the evolution of the moving boundaries. In particular, at the leading and trailing edge of the cell the velocity is determined by the vector sum, projected along the direction of motion, of the cytoskeleton material velocity and the polymerization and depolymerization velocity of the lamellipodial branched actin network (see Fig. 2), so that

$$\dot{a}(t) = -v_{pol}(a(t)) + v(a(t)) = -v_{pol}(a(t)) + \frac{1}{\beta}\frac{\partial \sigma}{\partial x}\bigg|_{a(t)}, \tag{5a}$$

$$\dot{b}(t) = v_{pol}(b(t)) + v(b(t)) = v_{pol}(b(t)) + \frac{1}{\beta}\frac{\partial \sigma}{\partial x}\bigg|_{b(t)}, \tag{5b}$$

where the fact that $v$ is given by Eq. (1) was used and an expression for the velocity of polymerization along the outward normal to the boundary, $\mathbf{v}_{pol} = v_{pol}\mathbf{n}$, has to be determined in order to close the system. We remark that, by convention, $v_{pol}$ is positive when the polymerization velocity is directed toward the outside of the cell [i.e., the edge located in $b(t)$ moves towards the right, whereas the boundary in $a(t)$ moves towards the left].

As observed in the introductory section, the basis for cell shape changes and migration is the polymerization of actin filaments in the protruding regions of the cell and the disassembly of these filaments in the regions of the cell being withdrawn. The whole process, at the subcellular level, depends on the flow of free and lamellipodial branched actin network. The G-actin monomers can freely diffuse inside the cytosol (i.e., they are passively transported by Brownian motion from regions of higher to regions of lower concentration) and can attach to the barbed ends of the growing branched actin network inside the lamellipodium. Then the newly polymerized actin is backward transported by the myosin motors (actin retrograde flow) until it disassembles inside the body of the cell. So, if there is not enough polymerization at the border of the cell, its border retracts ($\dot{b} < 0$), otherwise it advances. Without going through the microscopic description of the mechanisms and the different actin types involved in this complex process, which are still under study from the biological point of view [16], we here propose a modification of the minimal theoretical model proposed in Ref. [37], where only the influence of stress on actin dynamics has been considered, in order to include the effect of intracellular signaling molecules (that might also be an inhibitor of capping proteins), here denoted by $c(x,t)$, on the overall process. In particular, we focus on the fact that the presence of this polymerizing factor $c$ favors the formations of lamellipodial branched actin network recruiting and assembling actin monomers. The other types of actin filaments involved in different cell functions [16] are assumed in equilibrium with the monomer concentration. The lamellipodial polymerized actin anchors to the substrate at the leading edge of the cell and is transported at the velocity $v$ by the rest of the actin network due to the action of myosin motors, whereas the monomeric free actin diffuses inside the cytosol (considered at rest with respect to the substrate) with diffusion coefficient $D_a$, down the concentration gradient towards the cell leading edge (that acts as a sink for the G-actin [66]) where it finally attaches to the polymeric filaments. Therefore, considering a closed system, the concentration of globular actin, called $m$, and the concentration of lamellipodial filamentous actin, denoted by $p$, obey the following equations:

$$\frac{\partial m}{\partial t} - D_a \frac{\partial^2 m}{\partial x^2} = -\Psi(m, p, c, \sigma), \tag{6}$$

$$\frac{\partial p}{\partial t} + \frac{\partial}{\partial x}(pv) = \Psi(m, p, c, \sigma), \tag{7}$$

where $\Psi(m, p, c, \sigma)$ is the net assembly and disassembly rate of filamentous actin, and consequently the net loss and production rate of globular actin. In general the assembly and disassembly rate $\Psi(m, p, c, \sigma)$ definitely depends on the availability of actin monomers (that can polymerize at the barbed ends when they are not capped), on the presence of actin filaments (that can depolymerize), and it might be possibly determined either by the polymerizing factors, with dimensionless concentration $c(x)$ (scaled with respect to a characteristic reference concentration that will be specified in the simulations) [25,67], or by the stress inside the cell (since G-actin monomers detach in the body of the cell with a rate proportional to the stress [13,68]). Even though the effect of the internal stress on the polymerization and depolymerization process has been widely investigated [37,68], the influence of internal signaling molecules, which are fundamental, for instance, during chemotaxis, has been poorly investigated. Thus, without going into details, since the primary intracellular chemical activator has not been fully identified [69], we here consider a generic polymerizing factor $c$ which is responsible of the mechanism of actin-network assembly and disassembly. The expression of the polymerizing factor $c$ can be triggered by different external cues [18,19], such as the chemical field or the stress, as well as internal cues, such as random processes. The effect of all these stimuli on the polymerizing factor does not affect the validity of the present model and can be included *a posteriori*, as we will see in Sec. III F. Namely, we can set $\Psi(m, p, c, \sigma) \equiv \Psi(m, p, c)$ in Eqs. (6) and (7).

In particular, we here assume that actin polymerization occurs in presence of monomers availability and when the polymerizing factor $c(x,t) > c_{pol}$, whereas actin polymers (if available) disassemble when $c(x,t) < c_{pol}$, thus, setting

$$\Psi(m, p, c) = k_1(c - c_{pol})_+ m - k_{-1}(c_{pol} - c)_+ p, \tag{8}$$

where the parameters $k_1$ and $k_{-1}$ are the polymerization and depolymerization rate, respectively, and $(\cdot)_+$ stands for the positive part of its argument. The expression chosen for $\Psi(m, p, c)$ takes into account the *thresholding* mechanism [6], achieved at the level of second messengers, that enables us to determine the minimum level of signal necessary to activate the downstream response. The dependency of the polymerization velocity and possibly of other parameters in the model (such as the contractile active stress or the frictional parameter) on polymerizing factor availability requires one to determine its concentration inside the cell, which can be described by a standard reaction-diffusion equation

$$\frac{\partial c}{\partial t} - D_c \frac{\partial^2 c}{\partial x^2} = -\gamma c, \quad \text{for } a(t) < x < b(t), \tag{9}$$

where $D_c$ is the diffusion coefficient of the chemical and $\gamma$ is its decay rate. We remark that the spatiotemporal evolution of $c$ can be very different from that of the possible external chemical field, so that the cell can amplify the outer signal $n$, achieving steep internal gradients of signaling molecules (*amplification* mechanism [6]). Furthermore, the internal signal $c$ might be activated also in the absence of external factors. Proper boundary conditions should be provided in order to fulfill the description of the chemical signal. In particular, we assume that the concentration of the polymerizing factor at the boundary can be taken constant:

$$c(a(t)) = c_a, \qquad c(b(t)) = c_b. \tag{10}$$

Certainly, the values of $c_a$ and $c_b$ are related to the chemoattractant concentration $n$ in $a(t)$ and $b(t)$, respectively, or

eventually to other external cues. However, this dependency will not affect the validity of the BCs (10), and the link between the intracellular signaling molecule and the external chemical field will be discussed in Sec. III F. Finally, in order to solve the system, proper BCs for Eqs. (6) and (7) and the expression for the velocity $v_{pol}$ appearing in Eqs. (5) have to be provided. We consider that the free velocity of polymerization and depolymerization at the leading and trailing edge is directed along the outward normal to the cell boundary $\mathbf{n}$, and it is proportional to the net assembly and disassembly rate of filamentous actin, through the factor $\delta$, which is the length increment due to the addition of a $\mu$M of actin monomer to the existing network. Thus we set

$$\mathbf{v}_{pol} = \delta\Psi(m, p, c)\mathbf{n}. \tag{11}$$

Then the boundary conditions for the monomeric actin can be obtained by requiring the conservation of the total actin mass,

$$0 = \frac{d}{dt}\int_{a(t)}^{b(t)} (m+p)\,dx = \int_{a(t)}^{b(t)} \frac{\partial}{\partial t}(m+p)\,dx + \dot{b}(m+p)|_{b(t)} - \dot{a}(m+p)|_{a(t)},$$

which, recalling (6) and (7), is satisfied by nullifying the actin flux in $a(t)$ and $b(t)$, respectively:

$$[v(a(t)) - \dot{a}(t)]p(a(t)) - D_a \frac{\partial m}{\partial x}\bigg|_{a(t)} - \dot{a}(t)m(a(t)) = 0, \tag{12a}$$

$$\big[v(b(t)) - \dot{b}(t)\big]p(b(t)) - D_a \frac{\partial m}{\partial x}\bigg|_{b(t)} - \dot{b}(t)m(b(t)) = 0. \tag{12b}$$

Equations (12), together with (11), lead to the following boundary conditions for the monomeric actin:

$$\frac{\partial m}{\partial x}\bigg|_{a(t)} = \frac{1}{D_a}\left[-\frac{1}{\beta}\frac{\partial \sigma}{\partial x}m + \delta\Psi(m, p, c)(m+p)\right]\bigg|_{a(t)}, \tag{13a}$$

$$\frac{\partial m}{\partial x}\bigg|_{b(t)} = \frac{1}{D_a}\left[-\frac{1}{\beta}\frac{\partial \sigma}{\partial x}m - \delta\Psi(m, p, c)(m+p)\right]\bigg|_{b(t)}. \tag{13b}$$

Finally, concerning the polymeric actin involved in lamellipodia formation, due to the hyperbolic nature of Eq. (7), in order to find a unique solution, we have to impose BCs on the entry boundaries, i.e., where $(\mathbf{v}(x,t) - \mathbf{V}(x,t)) \cdot \mathbf{n}(x) \leqslant 0$, with $\mathbf{V}(x,t)$ the velocity of the cell boundary. Thus, with

$$\begin{aligned}[\mathbf{v}(a(t)) - \mathbf{V}(a(t))] \cdot \mathbf{n}(a(t)) &= -v(a(t)) + \dot{a}(t)\\ &= -v_{pol}(a(t)),\\ [\mathbf{v}(b(t)) - \mathbf{V}(b(t))] \cdot \mathbf{n}(b(t)) &= v(b(t)) - \dot{b}(t)\\ &= -v_{pol}(b(t)),\end{aligned}$$

the BC should be prescribed on $a(t)$ when $v_{pol}(a(t)) \geqslant 0$ and on $b(t)$ when $v_{pol}(b(t)) \geqslant 0$ (i.e., when $\mathbf{v}_{pol}$ is directed toward the outside of the cell). In particular, we assume that the concentration of filamentous actin at the boundary is proportional through $\alpha$ to the rate of polymerization of monomers at the corresponding boundary:

$$p(b(t)) = \alpha k_1 (c_b - c_{pol})_+ m(b(t)) \quad \text{if} \quad v_{pol}(b(t)) \geqslant 0, \tag{14a}$$

$$p(a(t)) = \alpha k_1 (c_a - c_{pol})_+ m(a(t)) \quad \text{if} \quad v_{pol}(a(t)) \geqslant 0. \tag{14b}$$

Thus the problem of cell motion is totally defined by Eqs. (3), (6), (7), and (9), coupled with the boundary conditions (4), (5), (10), (13), and (14).

In particular, taking $\chi$ and $\beta$ independent on the polymerizing factor and on the stress, it is possible to decouple Eqs. (3) and (9) from the rest of the system. Then the solution of Eq. (3) supplemented with BCs (4) can be analytically computed, leading to

$$\sigma(x,t) = -[\chi + k(L(t) - L_0)]\frac{e^{\sqrt{\frac{\beta}{\mu}}[b(t)-x]} + e^{\sqrt{\frac{\beta}{\mu}}[x-a(t)]}}{1 + e^{\sqrt{\frac{\beta}{\mu}}L(t)}} + \chi \tag{15}$$

so that the velocities of the boundaries are

$$\dot{a}(t) = \frac{\chi + k[L(t) - L_0]}{\sqrt{\beta\mu}} \tanh\left(\sqrt{\frac{\beta}{\mu}}\frac{L(t)}{2}\right) - v_{pol}(a(t)), \tag{16a}$$

$$\dot{b}(t) = -\frac{\chi + k[L(t) - L_0]}{\sqrt{\beta\mu}} \tanh\left(\sqrt{\frac{\beta}{\mu}}\frac{L(t)}{2}\right) + v_{pol}(b(t)). \tag{16b}$$

Furthermore, in a first approximation, it is possible to assume that the polymerizing factor diffuses much faster than the border expansion, so that the time-derivative term in Eq. (9) can be neglected, and the quasistationary chemical concentration field inside the cell is given by

$$c(x,t) = c_a \operatorname{csch}\left(\frac{L(t)}{\ell_c}\right)\sinh\left(\frac{b(t)-x}{\ell_c}\right) + c_b \operatorname{csch}\left(\frac{L(t)}{\ell_c}\right)\sinh\left(\frac{x-a(t)}{\ell_c}\right), \tag{17}$$

where $\ell_c = \sqrt{D_c/\gamma}$ is the diffusive length of the polymerizing factor. On the other hand, Eqs. (6) and (7) do not admit analytical solutions, and thus they should be solved numerically.

## III. NUMERICAL RESULTS

In this section, we simulate cell motion guided by actin polymerization in response to the internal polymerizing factor, by numerically solving the system of Eqs. (2), (6), (7), and (9) with boundary conditions (4), (10), (13), and (14) on the domain $[a(t), b(t)]$ whose boundaries move according to Eqs. (5). We consider the following biologically relevant conditions, neglecting, in a first instance, the upstream reasons of this phenomenon:

(1) The polymerizing factor is the same at both cell ends and above the threshold that can induce cell polymerization

TABLE I. Biologically meaningful ranges for the model parameters.

| Parameter | Description | Values | Ref. |
|---|---|---|---|
| $\chi$ | Active contractile stress | $10^2$–$10^3$ pN/$\mu$m$^2$ | [39] |
| $\mu$ | Cell's viscosity coefficient | $10^4$–$10^5$ pNs/$\mu$m$^2$ | [12,39] |
| $\beta$ | Cell-substrate friction coefficient | $10^3$–$10^5$ pNs/$\mu$m$^4$ | [12,39] |
| $L_0$ | Cell reference length | 10 $\mu$m | [39] |
| $k$ | Cell membrane elasticity | $10^2$ pN/$\mu$m$^3$ | [72] |
| $V$ | Cell characteristic speed | 10–30 $\mu$m/min | [5,12,15] |
| $v$ | Retrograde flow velocity at the cell front | 1–6 $\mu$m/min | [12,14,15] |
| $D_a$ | Actin monomers' diffusion coefficient | 3–30 $\mu$m$^2$/s | [5,12,75] |
| $\ell_c$ | Diffusion length of the intracellular signaling molecule | 1–5 $\mu$m | [69,76] |
| $p$, $m$ | Polymerized and unpolymerized actin | 100–300 $\mu$M | [12,75] |
| $k_1$ | Polymerization kinetic rate | [s$^{-1}$] | – |
| $k_{-1}$ | Depolymerization kinetic rate | [s$^{-1}$] | – |
| $\delta$ | F-actin elongation | $0.03/k_1$ $\mu$m/($\mu$Ms) | [75] |

$c_a = c_b > c_{pol}$ (the *symmetric polymerization* case); this condition can be induced, for example, by an homogeneous and abundant external chemical concentration, in the absence of other perturbing factors or spontaneous polarity.

(2) The polymerizing factor is the same at both cell ends and below the polymerization threshold, $c_a = c_b < c_{pol}$ (the *symmetric depolymerization* case), so that it is insufficient to trigger the protrusion of lamellipodia. This situation might correspond to an homogeneous distribution of external factors (such as chemoattractant or chemorepellent), in the absence of internal symmetry-breaking signals.

(3) The polymerization factor is higher at the cell front located in $b(t)$ than at the cell rear, i.e., either $c_a \leqslant c_{pol} < c_b$ or $c_{pol} < c_a < c_b$ (the *polarization and asymmetric polymerization* case). This last condition can be triggered, for instance, by the profusion of chemoattractant at the leading front and its scarceness at the trailing edge, but it can also be related to a spontaneous polarization of the cell that produce an asymmetry in the polymerizing factor.

For sake of completeness, we also discuss the remaining asymmetric cases, specifically $c_a < c_b < c_{pol}$ (the *asymmetric depolymerization* case), at the end of Sec. III D. Finally, in Sec. III F, we study, with particular reference to chemotaxis, the possible relationship between the intracellular polymerizing factor $c$ and the extracellular chemical field $n$, and we discuss the related consequences on cell motion.

### A. Numerical method

The simulations presented in this section have been obtained using MATLAB (MathWorks, Natick, MA).

Since we have to deal with a moving segment, we mapped the equations of the system onto a fixed domain [0, 1]. To this end, we introduced the new space variable

$$y = \frac{x - a(t)}{L(t)} \in [0, 1],$$

and we rewrote all equations with respect to the comoving frame. The internal chemical signal was assumed at the steady state, so that we used the analytic expression given by Eq. (17), written with respect to the new space variable, to compute the polymerizing factor distribution. Also the stress field inside the comoving frame can be analytically computed, by properly rescaling Eq. (15) with respect to the comoving variable. On the other hand, the distributions of the actin monomers and filaments are computed by discretizing the corresponding Eqs. (6) and (7), written with respect to the space variable $y$, using a finite difference scheme. Specifically, spatial diffusion terms, which contain the second derivatives, are approximated by central differences in space, convective terms are discretized using an upwind scheme, and an explicit Euler scheme was used to model the evolution in time. The discretization size on the fixed grid was set to be equal to $\Delta y = 0.005$, and the time interval $\Delta t$ for each time step was adapted to ensure that the Courant-Friedrichs-Lewy condition and the requirement $\Delta t < \Delta y/(2D_c)$ are satisfied.

### B. Parameter estimation

The admissible ranges of values for the model parameters are listed in Table I, as extracted from the literature. Since biological data on the polymerizing factors are not available, we considered its concentration to be dimensionless with respect to the intracellular chemical signal at the leading edge, so that $c_b = 1$. The active contractile stress $\chi = 10^2$–$10^3$ pN/$\mu$m$^2$ [39] can be inferred by measurements of the traction force per unit area exerted by the cell on the surface of adhesion, which can be experimentally obtained with a variety of methods [70,71]. The viscosity coefficient of the cell described as an active gel, can be estimated from the cell's elastic modulus and the characteristic time of relaxation [12,39], leading to $\mu \approx 10^4$–$10^5$ pNs/$\mu$m$^2$. Even though the friction coefficient $\beta$, associated with cell adhesion to the surface, has not been measured directly, its order of magnitude has been estimated to be $\approx 10^3$–$10^4$ pNs/$\mu$m$^4$ in Ref. [39] and $\approx 3 \times 10^4 - 10^5$ pNs/$\mu$m$^4$ in Ref. [12], considering a lamellipodial thickness ranging from 0.17 $\mu$m [5] up to 1 $\mu$m [12]. Furthermore, considering the elastic modulus of a cell membrane reported in [72] for a cell with reference length $L_0 = 10$ $\mu$m [39] it is possible to estimate $k = 10^2$ pN/$\mu$m$^3$, although recent experiments on supported lipid bilayers [73], which are valid biomimetic systems for the study of membrane biophysical properties, suggest that cell membrane elastic modulus could be still larger, possibly leading to higher

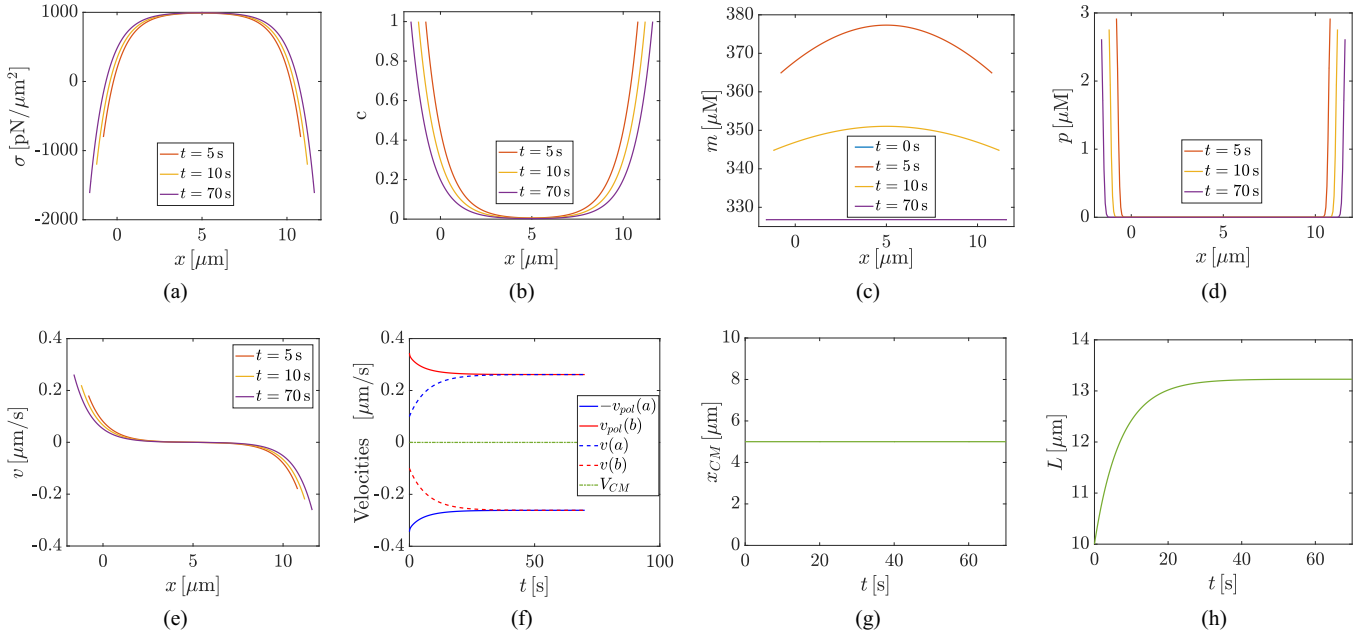


FIG. 3. Spatial evolution at several times of (a) the stress $\sigma$, (b) the intracellular polymerizing factor $c$, (c) the monomeric actin $m$, (d) the lamellipodial polymeric actin $p$, and (e) the actin network velocity $v$. Temporal evolution of (f) the velocities of polymerization at the two ends (red and blue solid line), the velocity of the free boundaries (red and blue dashed line) and the velocity of the center of mass (green dotted line), (g) the position of the center of mass of the cell, and (h) the cell length, when the concentration of chemicals is above $c_{pol}$ in both $a(t)$ and $b(t)$. In the simulation we set $a(0) = 0\,\mu\mathrm{m}$, $b(0) = 10\,\mu\mathrm{m}$, $L_0 = 10\,\mu\mathrm{m}$, $\chi = 10^3\,\mathrm{pN}/\mu\mathrm{m}^2$, $\beta = 10^4\,\mathrm{pNs}/\mu\mathrm{m}^4$, $\mu = 10^4\,\mathrm{pNs}/\mu\mathrm{m}^2$, $k = 500\,\mathrm{pN}/\mu\mathrm{m}^3$, $c_b = c_a = 1$, $c_{pol} = 0.98$, $D_c = 1\,\mu\mathrm{m}^2/\mathrm{s}$, $\gamma = 1s^{-1}$, $D_a = 10\,\mu\mathrm{m}^2/\mathrm{s}$ $\alpha = 0.5\,\mathrm{s}$, $k_{-1} = 50\,\mathrm{s}^{-1}$, $k_1 = 0.8\,\mathrm{s}^{-1}$, $\delta = 5 \times 10^{-2}\,\mu\mathrm{m}/\mu\mathrm{M}$, $m_b = 430\,\mu\mathrm{M}$, $m_a = 430\,\mu\mathrm{M}$, $p_b = \alpha k_1 (c_b - c_{pol})_+ m_b$, $p_a = \alpha k_1 (c_a - c_{pol})_+ m_a$.

values of the parameter $k$. The characteristic speed and final size of the cell can be directly measured from experiments on a specific cell type, e.g., fish keratocytes move with a velocity of a few tens of $\mu$m/min (up to 1 $\mu$m/s) [5,12,15,74] and have a length of few tens of $\mu$m.

For what concerns the dynamics of actin filaments, the diffusion coefficient of actin monomers has been estimated to be $D_a \approx 3$–$30\,\mu\mathrm{m}^2/\mathrm{s}$ [5,12,75], whereas the retrograde flow at the cell front ranges between $\approx$1–6 $\mu$m/min [12,14,15]. On the other hand, the effective kinetic rates $k_1$ and $k_{-1}$ for the proposed model of polymerization are unknown, since the underlying biochemical reactions for actin polymerization and depolymerization can be really complex, involving a variety of multistep reactions and subproducts [5,75]. Therefore in the simulations we varied them a few orders of magnitude, and in Table I we report only their descriptions and units of measure. At the same time the parameter $\delta$ which represents the length increment for filamentous actin, when 1 $\mu$M of monomeric actin binds to the barbed ends, has not been experimentally measured.

A possible way to estimate $k_1$ and $\delta$ is to consider the exceptionally fast elongation rates of barbed ends in diluted buffers, which is $\approx$0.3–3 $\mu$m/s for a concentration of unpolymerized actin of 10–100 $\mu$M [75]. Thus, for the proposed polymerization velocity, considering for sake of simplicity $c_{pol} = 0$, we have $k_1\delta = 0.03\,\mu\mathrm{m}/(\mu\mathrm{Ms})$. We remark that this conjecture has been formulated only to obtain a physically admissible estimation of these parameters, and for $c_{pol} > 0$ the value of $k_1\delta$ should be greater than $0.03\,\mu\mathrm{m}/(\mu\mathrm{Ms})$ in order to obtain the same polymerization velocity.

Given the different types of filamentous and globular actin that coexist in cells, it is not currently feasible to experimentally measure the actin concentration profile across the lamellipod [5]. However, from indirect information, it is possible to estimate that the polymerized and unpolymerized actin ranges between 100–1000 $\mu$M [5,12,75]. However, a large pool of actin monomers can be sequestered by actin-binding proteins in a form unavailable for polymerization, and thus also lower concentration can be found in literature ($\approx$30–40 $\mu$M) [5], and the lamellipodial branched actin concentration can be sensitively lower than the reported concentration for the whole polymerized actin network. The intracellular second messenger, here called polymerizing factor, that is produced on the activation of chemoattractant receptors should not be allowed to diffuse very far into the cell in order to establish and preserve a front-to-tail polarity, and at the same time it must diffuse over some distance to locally integrate information from several occupied receptors and preserve cell ability to detect shallow gradients [69,76]. The polymerizing factor diffusion is totally defined, as shown at the end of Sec. II, by a single parameter: the diffusion length, $\ell_c = \sqrt{D_c/\gamma}$, which describes the average distance that a signaling molecule with diffusion coefficient $D_c$ travels from its source before it is degraded after a lifetime of $\gamma^{-1}$. Thus, the capacity of this intracellular factor to establish and maintain localized signals is actually determined by its diffusion length, which must be small compared to the cell length, but not too much. In particular, soluble second messengers (e.g., cGMP) with diffusive lengths of the order of tens of $\mu$m cannot preserve spatial information [69], whereas transmembrane proteins

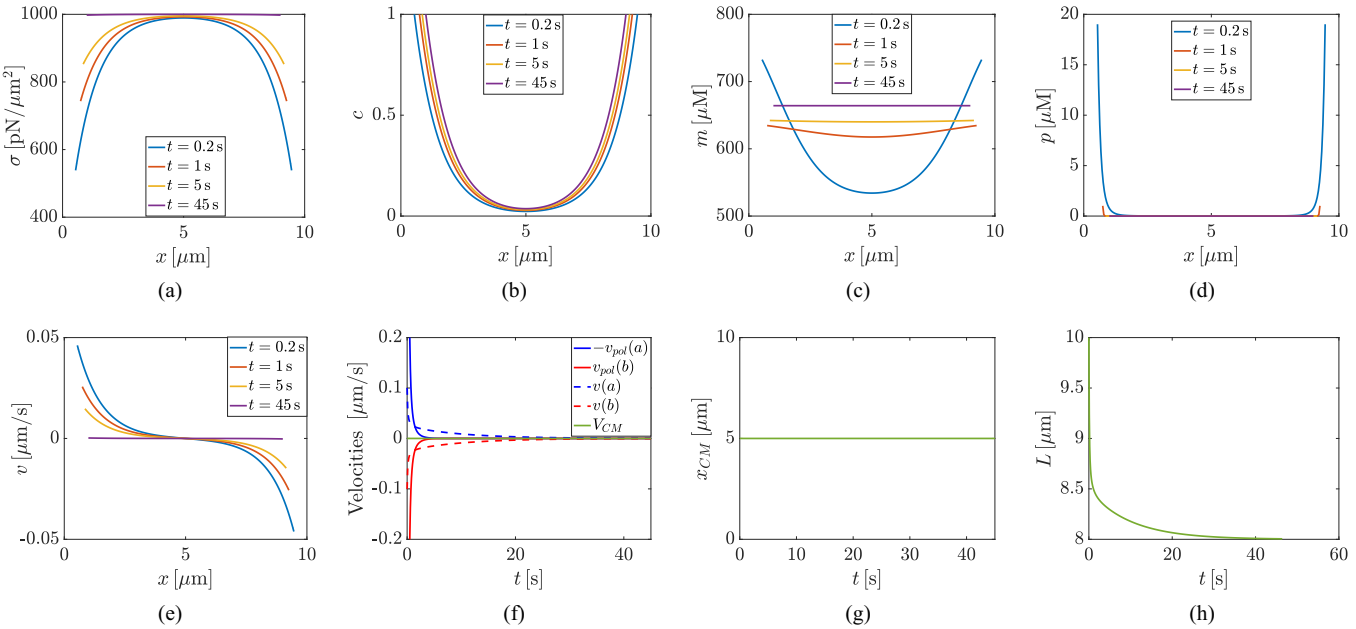


FIG. 4. Spatial evolution at several times of (a) the stress $\sigma$, (b) the intracellular polymerizing factor $c$, (c) the monomeric actin $m$, (d) the lamellipodial polymeric actin $p$, and (e) the actin network velocity $v$. Temporal evolution of (f) the velocities of polymerization at the two ends (red and blue solid line), the velocity of the free boundaries (red and blue dashed line) and the velocity of the center of mass (green dotted line), (g) the position of the center of mass of the cell, and (h) the cell length, when the concentration of chemicals is below $c_{pol}$ in both $a(t)$ and $b(t)$ (color online). In the simulation we set the same parameters as in Fig. 3, except for $c_a = 1$ and $c_{pol} = 1.02$.

such as receptors (e.g., cAMP-receptor complex) diffuse extremely slowly with diffusive lengths of the order of the closest receptor distance (i.e., $\ell_c = 0.2\,\mu$m) [69]. Therefore, second messengers with diffusion length in the order of $\ell_c = 1 - 5\,\mu$m are the most efficient in setting a suitable internal chemical signal and acting as polymerizing factors [76].

### C. Symmetric polymerization and depolymerization case

When the concentration of the polymerizing factor at both cell ends is the same, i.e., in either the symmetric polymerization or depolymerization cases (Figs. 3 and 4, respectively), the total displacement of the center of mass [see Fig. 3(g) and Fig. 4(g)] is nearly equal to zero, and thus the cell does not actually move, even though it can shrink or stretch itself. In both cases the cell reaches a stationary condition, with a final length which is slightly higher [Fig. 3(h)] or lower [Fig. 4(h)] than the reference length $L_0$, depending on whether $c_{pol} < c_a = c_b = 1$ or $c_{pol} > c_a = c_b = 1$. This result is in accordance with biological experiments performed on *Dictyostelium* and neutrophil cells [19], that when stimulated in a uniform manner (e.g., the entire membrane is equally accessible to chemoattractant or mechanical stimulants) and in the absence of spontaneous polarization, grow and retract protrusions stochastically throughout the plasma membrane. Thus, even when polymerization occurs, cells do not move because they cannot form successive protrusions at a single site on the membrane, thus the cell body is not displaced towards a single direction.

Furthermore, throughout the simulations, the stress $\sigma$, the polymerizing factor $c$, the polymeric actin $p$ involved in lamellipodia formation, and the monomeric actin $m$ are symmetric with respect to the center of mass of the cell [Figs. 3(a)–3(d) and Figs. 4(a)–4(d)], with the field distributions highly dependent on whether actin assembly or disassembly occurs. Specifically, in the polymerization with no motion case, the stress is compressive close to the cells ends, due to membrane resistance to cell elongation, whereas it is positive inside the cell because of the active myosin contraction [see Fig. 3(a)]. For what concerns the polymerizing factor, in this case, for the chosen values of $D_c$ and $\gamma$, since $\ell_c = 1\,\mu$m, there is only a small portion close to the cell ends where $c(x,t) > c_{pol}$ [Fig. 3(b)], and thus polymerization can effectively occur. Consequently, the monomers concentration at the steady state is higher inside the cell and lower closer to the cell boundaries [Fig. 3(c)], due to continuous filaments assembly, that leads to a peak in the polymeric actin at both cells ends, denoting the formation of lamellipodia, as shown in Fig. 3(d). We observe that, with $p$ the concentration of lamellipodial actin filaments, we correctly have $p$ nearly equal to zero in the center of the cell. Indeed, the lamellipodial actin population is merely observed at the leading edge of the cell and disappears abruptly about 1–3 $\mu$m back [17]. The lamellipodial actin also exhibits rapid retrograde flow (with respect to the lamellar actin population) [17]. Thus, even though, at the steady state, the polymeric actin cytoskeleton close to the cell ends grows at a constant rate, it is back-transported from the boundary to the interior (backward flow) at the same velocity it is produced [see Fig. 3(f)], so that the total displacements of the cell ends vanish.

On the other hand, in the symmetric depolymerization case, the contractile stress inside the cell is positive and homogeneously distributed [Fig. 4(a)], since the membrane tension also acts to restore the reference length of the cell, while depolymerization of lamellipodial actin inexorably occurs until, at the steady state, $p$ is null everywhere [Fig. 4(d)], since

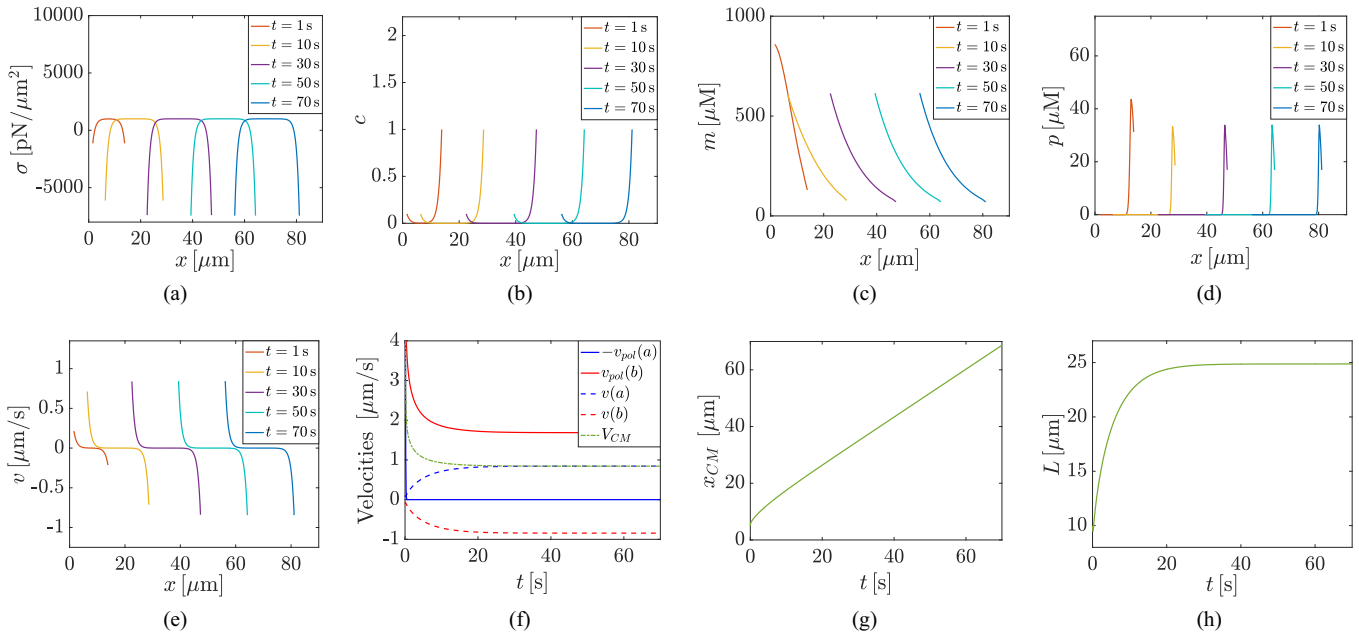


FIG. 5. Spatial evolution at several times of (a) the stress $\sigma$, (b) the polymerizing factor $c$, (c) the monomeric actin $m$, (d) the lamellipodial polymeric actin $p$, and (e) the actin network velocity $v$. Temporal evolution of (f) the velocities of polymerization at the two ends (red and blue solid line), the velocity of the free boundaries (red and blue dashed line) and the velocity of the center of mass (green dotted line), (g) the position of the center of mass of the cell, and (h) the cell length, when $c_a < c_{pol} < c_b$ (i.e., the cell moves to the right). In the simulation we set the same parameters as in Fig. 3, except for $c_b = 1$, $c_a = 0.1$, and $c_{pol} = 0.4$.

$c(x,t) < c_{pol}$ in the whole cell [Fig. 4(b)]. The concentration of globular actin $m$ inside the cell increases to satisfy the mass conservation constraint [Fig. 4(c)]. In this case, at the steady state neither polymerization [being $c(x,t) < c_{pol}$] nor depolymerization [being $p(x,t) \equiv 0$] occurs, and the actin flow is null everywhere, $v(x,t) \equiv 0$, since the stress is constant inside the cell [Fig. 4(e)].

### D. Polarization and asymmetric polymerization

The most interesting case occurs when the cell is polarized, and, in our conjecture, this polarity can then be represented by an asymmetry in the boundary conditions for the polymerizing factor $c$, which in turn can be either related to external cues or spontaneously generated. For instance, an asymmetry in the intracellular polymerizing signaling can be induced when the cell senses an external chemical gradient, i.e., when the concentration of the chemoattractant or chemorepellent $n(x,t)$ on one cell end is higher than at the opposite boundary. In this case, the imbalance of the internal signaling drives actin dynamics along with cell motion towards the highest external chemical concentration and eventual cell extension or shrinkage. Specifically, we consider the case in which the polymerizing factor concentration is higher in $b(t)$ than in $a(t)$, so that the cell end in $b(t)$ becomes the leading edge, whereas the opposite cell end turns into the trailing edge and the cell moves to the right. In particular, we consider either the case in which the intracellular polymerizing signaling can trigger lamellipodial actin assembly only at the leading edge, $c_a \leqslant c_{pol} < c_b = 1$ (see Fig. 5), and the case in which polymerization occurs both at the leading and at the trailing edge of the cell, $c_{pol} < c_a < c_b = 1$ (see Fig. 6). In both cases, as shown in Fig. 5(a) and Fig. 6(a), the stress field continues to be symmetric, with compressive stress at the boundaries due to cell extension and tension inside the cell body. This result is due to the assumption that the active stress is independent on the position and on the actin polymerization. Indeed, in the present formulation, the polarization dynamics and the stress pattern are fully decoupled, as done, for instance, in Ref. [37]: the stress field generated by an asymmetric acto-myosin pattern is not taken into account, as well as is not considered the influence of the mechanical stress on the polymerization process. This choice has been made in order to focus on the influence of internal chemical signaling on the whole migratory process, while the introduction of the coupling between the stress field on the acto-myosin concentration would have made the final results, for the perspectives of this work, less transparent.

On the other hand, the polymerizing factor field reflects the asymmetric boundary conditions, with a higher concentration of $c$ at the leading edge (where $c_b = 1$) and a concentration of the this intracellular signaling molecule in $a(t)$ below $c_{pol}$ in Fig. 5(b) and above it in Fig. 6(b). For the particular choice of $D_c$ and $\gamma$, in the simulations $\ell_c = 1\,\mu$m, accordingly to the biological range [69,76], so that the polymerizing factor rapidly decays inside the cell body and its action is mainly located at the cell periphery (i.e., either the leading edge in the case $c_a \leqslant c_{pol} < c_b = 1$ or both cell ends in the case $c_{pol} < c_a < c_b = 1$). Thus, Figs. 5(b) and 6(b) well represent the existence of a steep intracellular gradient of signaling molecules, which triggers the localized polymerization and depolymerization of actin at the cell boundaries, even when the external signal, such as the chemoattractant, gradient is not so pronounced [77]. The spatiotemporal evolution of

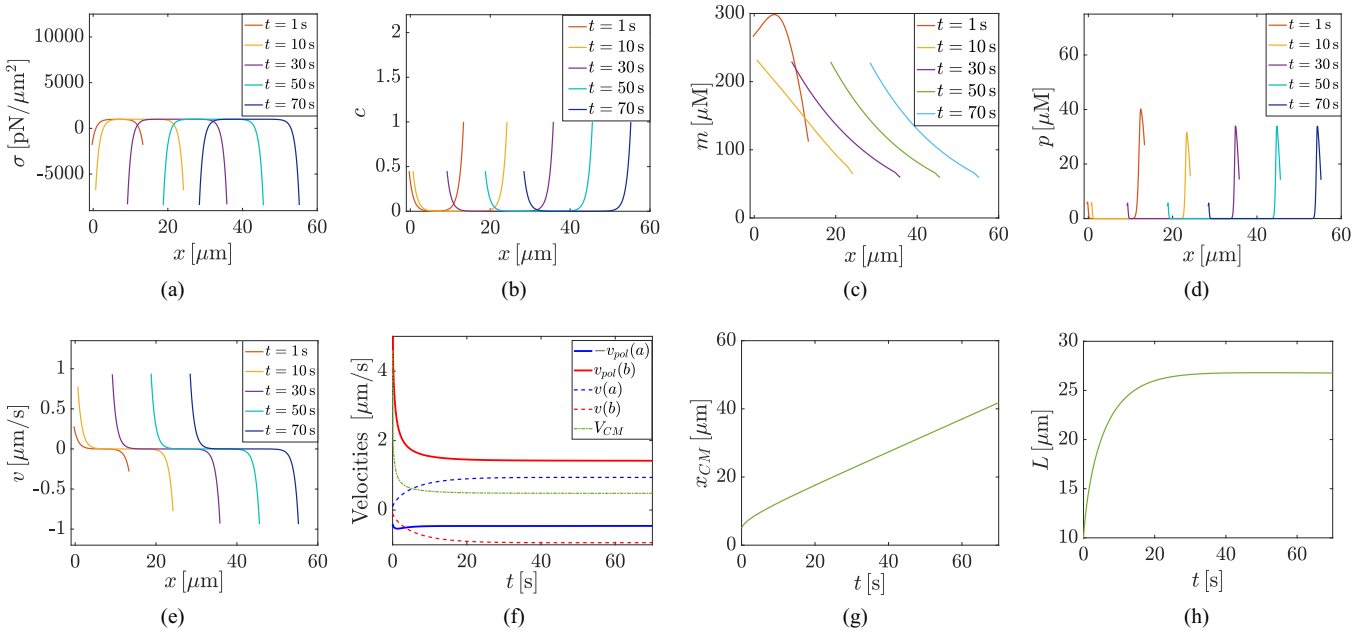


FIG. 6. Spatial evolution at several times of (a) the stress $\sigma$, (b) the polymerizing factor $c$, (c) the monomeric actin $m$, (d) the lamellipodial polymeric actin $p$, and (e) the actin network velocity $v$. Temporal evolution of (f) the velocities of polymerization at the two ends (red and blue solid line), the velocity of the free boundaries (red and blue dashed line) and the velocity of the center of mass (green dotted line), (g) the position of the center of mass of the cell, and (h) the cell length, when $c_{pol} < c_a < c_b$, i.e., polymerization occurs also at the cell rear. In the simulation we set the same parameters as in Fig. 5, except for $c_a = 0.45$.

the monomeric and lamellipodial polymeric actin fields is reported in Figs. 5(c) and 5(d) and Figs. 6(c) and 6(d), respectively. Independently of the chemical availability at the rear of the cell, the monomers concentration decreases from the trailing towards the leading edge [Fig. 5(c) and Fig. 6(c)]. However, in the case in which polymerization occurs also at the trailing edge (i.e., $c_{pol} < c_a < c_b = 1$), the monomers concentration inside the cell is lower than in the case in which depolymerization occurs at the rear of the cell. The lamellipodial actin concentration is higher at the cell front, with a maximum just behind the leading edge [Fig. 5(d) and Fig. 6(d)], and it rapidly decreases towards zero in the center of the cell. Whereas in the case in which $c_a \leqslant c_{pol} < c_b = 1$, the lamellipodial actin branched network forms only at the cell front [Fig. 5(d)], when filament assembly occurs also at the cell rear, we have another peak of lamellipodial actin at the trailing edge [Fig. 6(d)]. Finally, Fig. 5(e) and Fig. 6(e) report the actin network velocity evolution in time and space: $v$ is always retrograde at the leading edge (i.e., the actin flow moves in a direction opposite to the direction of cell motion with respect to the substrate) and anterograde at the trailing edge (actin and cell move in the same direction), in accordance with biological findings [12–15]. It is interesting to observe that, in both cases, the obtained solutions are of a traveling wave type: the velocity of the traveling wave [green dotted line in Fig. 5(f) and Fig. 6(f)], which is given by the slope of the curve representing the position of the center of mass over time [Fig. 5(g) and Fig. 6(g)], is higher in the case in which polymerization occurs only at the leading edge of the cell, whereas the length of the traveling segment, i.e., when the quasistationary configuration is reached, is reasonably higher in the case in which cell forms protrusions also at the trailing edge [Fig. 6(h) versus Fig. 5(h)]. Indeed, when $c_{pol} < c_a < c_b$, the polymerization pushes the membrane at the cell rear outward, and the velocity of polymerization along the direction of motion [i.e., $-v_{pol}(a)$] there is negative [blue solid line in Fig. 6(f)], leading to cell extending protrusion also at the rear.

For sake of completeness, we remark that when the polymerizing factor is below the threshold set for polymerization at both cell ends (the *asymmetric depolymerization* case), depolymerization occurs at both cell ends until, at the steady state, the concentration of $p$ is null everywhere in the cell, the cell does not move and has a length lower than the reference length $L_0$.

### E. Sensitivity analysis

In this section, we perform a sensitivity analysis, studying how the traveling wave solution varies as a function of the model parameters. Since the system of Eqs. (2), (6), (7), and (9) does not admit an analytical solution even when the traveling wave hypothesis is formulated, the effect of the different parameters on the solution of the system is studied numerically. In particular, Figs. 7 and 8 report the traveling wave velocity $V_{TW}$ (top row) and length $L_{TW}$ (bottom row) of the cell, changing one parameter at a time. They have been derived by numerically solving the model for each set of parameters and reporting the velocity of the center of mass $V_{CM}$ and the length of the cell $b(t) - a(t)$, when a traveling wave solution is numerically reached. In Fig. 7 the effect of the parameters related to cell mechanics is studied, whereas in Fig. 8 the influence of the parameters related to the chemical polymerization dynamics is considered. For

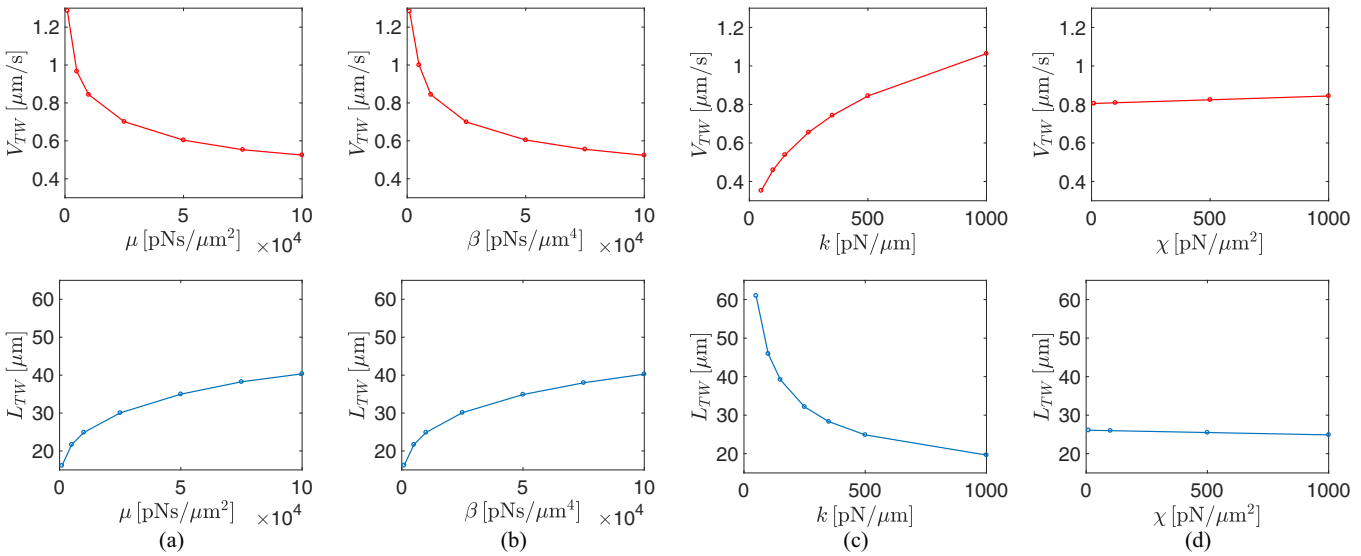


FIG. 7. Sensitivity analysis: in each panel we changed only the parameter reported in the horizontal axis, while keeping the others fixed (the values of the unchanged parameters is specified in the caption of Fig. 5). The charts report the traveling wave velocity (top of each subfigure) and length (bottom of each subfigure) changing the parameters (a) $\mu$, (b) $\beta$, (c) $k$, and (d) $\chi$. The traveling wave velocity, $V_{TW}$, and length, $L_{TW}$, have been derived by numerically solving the model to the steady state, for each set of parameters.

increasing values of the cell's viscosity coefficient $\mu$ and the cell-substrate friction coefficient $\beta$, the traveling wave velocity decreases, as expected from the theory, whereas the length of the traveling segment increases, up to four times the reference length $L_0$ [see Figs. 7(a) and 7(b)]. On the other hand, increasing values of the cell membrane elasticity $k$ makes the cell less extensible and speeds it up, as shown in Fig. 7(c). The active stress $\chi$ slightly influence, in an almost linear manner, the traveling wave cell velocity and length [Fig. 7(d)], at least in the range of parameters considered. We remark that the curves reported in Figs. 7(b) and 7(d) do not reflect the experimentally observed biphasic behavior [78–80] of cell speed dependency on the adhesion strength (that correlate with $\beta$ in the model) and on the level of myosin contraction (which is related to $\chi$ in our model), i.e., the cells crawl faster at low and high adhesion strengths when myosin activity is decreased or increased, respectively [78]. The simplest purely mechanical explanation for the biphasic migration-velocity response to increased adhesion strength is that, at low adhesion, contraction pulls weak focal adhesions at both the cell front and rear; at high adhesion, as well, contraction cannot overcome adhesion at the cell front or rear; on the other hand, at intermediate adhesion, an optimum is reached, with traction generated at the front coupled to

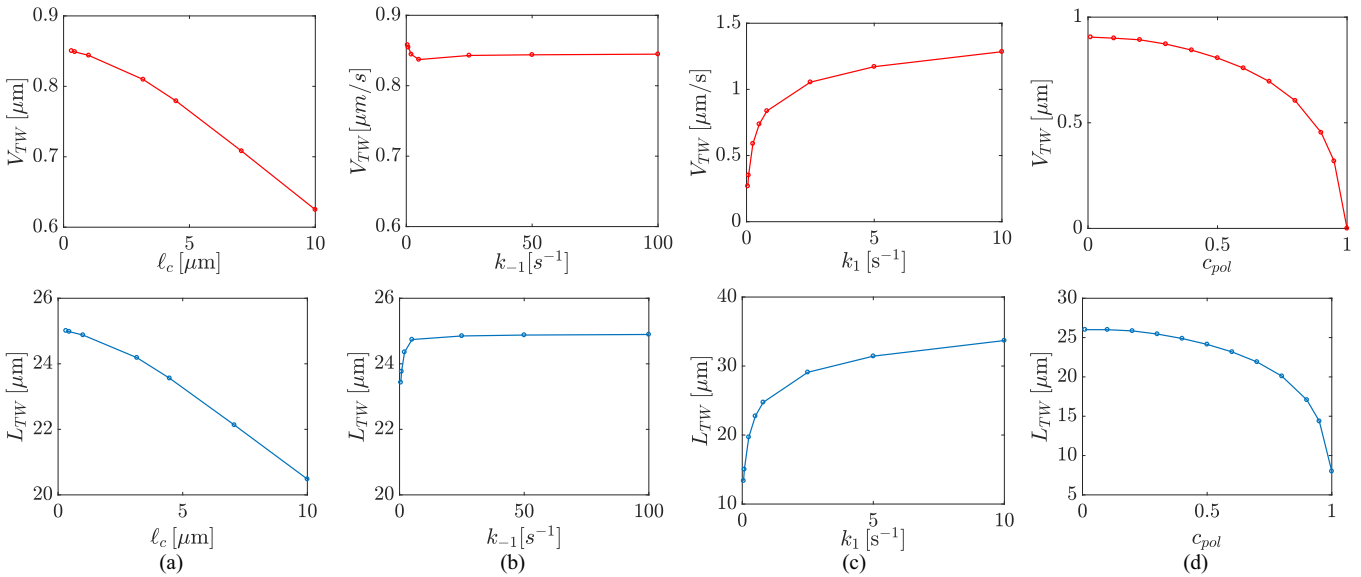


FIG. 8. Sensitivity analysis: in each panel we changed only the parameter reported in the horizontal axis, while keeping the others fixed (the values of the unchanged parameters is specified in the caption of Fig. 5). The charts report the traveling wave velocity (top of each subfigure) and length (bottom of each subfigure) changing the parameters (a) $\ell_c = \sqrt{D_c/\gamma}$, (b) $k_{-1}$, (c) $k_1$, and (d) $c_{pol}$.

adhesion detachment at the rear. This observation will be translated into a dependency of the the parameter $\chi$ on the the ability of the cell to bind to the substratum, which in turn regulates $\beta$ and the whole polymerization dynamics. Thus, the biphasic behavior is the outcome of a series of interrelated process, such as the dynamic organizational state of F-actin and focal adhesions and the myosin II distribution and activity in the contractile module [78]. All these factors in turns depend on the cell's ability to bind to the substrate, which can activate and alter different signal-transduction pathways. In carrying the sensitivity analysis, we preferred to keep all the parameters independent in order to change one parameter at a time, without including explicit relations between the different model parameters and the measurable biological quantities (e.g., adhesion strength, focal adhesion extension, ECM concentration, myosin, and actin distribution). Of course, this is a virtual setup which is unlikely to be reproduced experimentally, since in biological experiments changing a single factor will dramatically alter many cellular and subcellular mechanisms, most of them are even not known. Thus, the study of the dependency of the parameters $\beta$ and $\chi$ on the adhesion strength, acto-myosin distribution, and environmental conditions, along with the inclusion of mechanotransduction pathways (i.e., how adhesion strength and stresses act on the internal chemical signal $c$, regulating F-actin assembly and disassembly), are left for future investigations.

Focusing on the chemical parameters of the model, the numerical simulations confirm that the parameters $\gamma$ and $D_c$ simultaneously affect the traveling wave solution by changing the diffusive length of the intracellular signaling molecules, $\ell_c = \sqrt{D_c/\gamma}$. The results reported in Fig. 8(a) show that when the diffusive length increases the polymerization is less effective, with the polymerizing factor not clustered at the cell membrane, and thus the traveling cell length and velocity decreases for increasing values of $\ell_c$.

In the range of parameters considered, the kinetic rate of actin depolymerization $k_{-1}$ [Fig. 8(b)] slightly influences the traveling cell length ($\approx 2\,\mu$m increase in cell length for an increase of three order of magnitude in $k_{-1}$), and the traveling wave velocity (less than $0.02\,\mu$m/s decrease in cell velocity for an increase of three orders of magnitude in $k_{-1}$).

On the other hand, the traveling wave velocity and length are highly sensitive to the kinetic rate of actin polymerization $k_1$: as reported in Fig. 8(c), the velocity of the moving cell and its length increase proportionally to the logarithm of the parameter $k_1$.

Finally, as expected, the traveling wave velocity and length decrease when the threshold set for the polymerization $c_{pol}$ increases, since in this case the velocity of polymerization, which is proportional to the difference between $c$ and $c_{pol}$, is lower. In particular, for a very low value of the parameter $c_{pol}$ the cell velocity reaches a plateau, whereas when $c_{pol} > c_b = 1$ the cell does not move, since no polymerization occurs.

### F. Cell chemotactic velocity

Let us now link the intracellular polymerizing factor to the external chemical field, in order to plot the velocity curve shown in Fig. 8(d) with respect to the concentration of a chemoattractant, inducing cell motion. Without going into the details of the subcellular mechanisms involved in this complex process, in order to illustrate that intracellular mechanisms converting the chemotactic signal $n$ into the cell response can be included *a posteriori*, we here postulate different possible relationships between the polymerizing factor at the membrane $c_m(t)$ and the signal generated by activated receptors at the cell boundaries (here assumed to be directly related to the external chemical field), $n_m(t)$, with $m = \{a, b\}$. Indeed, as already stated, the internal chemical signal $c_m$ at the membrane is a response to extracellular chemoattractants perceived by transmembrane receptors, possibly mediated by the activation of protein cascades downstream, and, thus, it is not necessarily a linear amplification of the external signal [82]. In particular, in the following, we restrict our focus to two case studies:

(1) The concentration of the polymerizing factor at the cell membrane is proportional to the receptor signal and, consequently, to the chemoattractant field at the cell membrane see Fig. 9(a), top.

(2) The polymerizing factor is activated at the cell boundaries by the external chemical concentration through a complex molecular pathway holding inside the cell membrane and possibly leading to a bistable relation between $c_m$ and $n_m$, with $m = \{a, b\}$ [see Fig. 9(b), top].

Then in Fig. 9 (bottom), the traveling wave velocity is plotted as a function of a measure of the chemoattractant gradient sensed along the cell, defined as the ratio between the difference in the normalized chemoattractant concentration at the cell ends and the normalized cell traveling length. In particular we normalized the chemoattractant field $\bar{n}_m$ with respect to $c_{pol}$ and the cell length $L_{TW}$ with respect to $L_0$, so that the normalized external chemical field gradients reads $(\bar{n}_b - \bar{n}_a)/\bar{L} = [(n_b - n_a)L_0]/(c_{pol}\, L_{TW})$.

The linear relation between $c_m$ and $n_m$ [Fig. 9(a), top] leads to a cell velocity which can be said to increase linearly only for small values of the chemoattractant gradient, accordingly to the standard chemotactic relation [50]. However, for higher external chemical field gradients, it saturates [Fig. 9(a), bottom]. This behavior is reasonable from the biological point of view, since cell velocity cannot grow indefinitely high even when the cell is subject to an external chemical field with a really steep gradient. In fact, in the modeling literature nonlinear relations have been shown to best represent chemotaxis on a wide range of chemoattractant concentrations [49]. Furthermore, the predicted velocity versus chemical gradient curve is in good agreement with the data collected for migrating leukemia cancer Jurkat cells [62]. Indeed, the performed experiments highlight that the velocity rapidly increases when the gradient initially increases, and subsequently the cell velocity stabilizes to a maximum value. This phenomenon can be attributed to the saturation of the chemoattractant receptors at the cell membrane. We remark that the experimentally measured maximum velocity is of the order of $\approx 3\,\mu$m/min, which is slightly higher that the one reported in our work $\approx 0.9\,\mu$m/min.

The linear relationship postulated above, even though it allows to obtain a nonlinear relation between cell velocity and external chemical field due to the introduced mechanism of actin polymerization, is an unduly simplistic approximation of the true signal dynamics [82]. Indeed, as stated in the

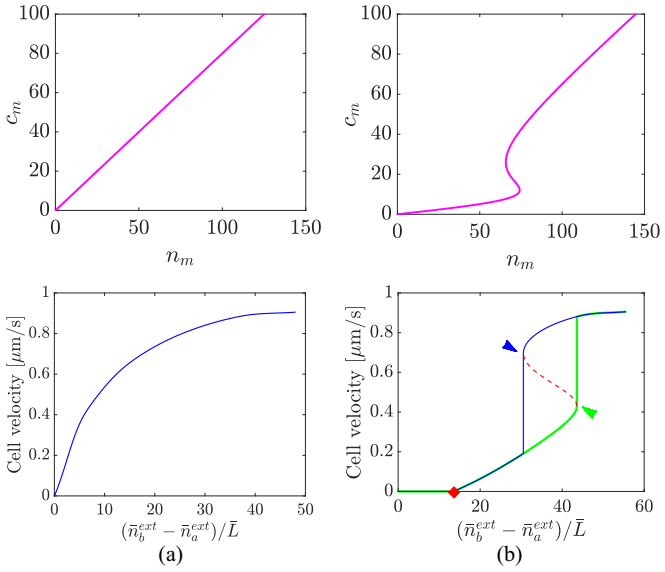


FIG. 9. Relation between the polymerizing factor $c_m$ ($m = \{a, b\}$) and the chemoattractant and receptor signal at the membrane $n_m$ (top) and cell traveling wave velocity as a function of the normalized gradient of the external chemical concentration (bottom) in the case in which we postulate either (a) a linear or (b) a bistable relation [through Eq. (20), setting $d = 2$ and, in order to minimize the number of required parameters, $\beta_c = \beta_i = 70\,\mathrm{s}^{-1}$, $\alpha_c = \alpha_i = 6\,\mathrm{s}^{-1}$, $K_c = K_i = 30$, $s_m = 70$]. We remark that, for this particular choice of parameters, the concentration of the intramembrane activator, $s_m$, is considered independent on the chemoattractant field, and thus it is set equal at both cell ends. The normalized gradient of the external chemical concentration is $(\bar{n}_b - \bar{n}_a)/\bar{L}$ where $(\bar{n}_b - \bar{n}_a) = (n_b - n_a)/c_{pol}$ and $\bar{L} = L/L_0$. The red (black) square diamond indicates the transition from the cell at rest to a moving cell, the green (light gray) pointed arrow indicates a transition to higher speed motion, conversely the pointed blue (dark gray) arrow denotes the reverse transition.

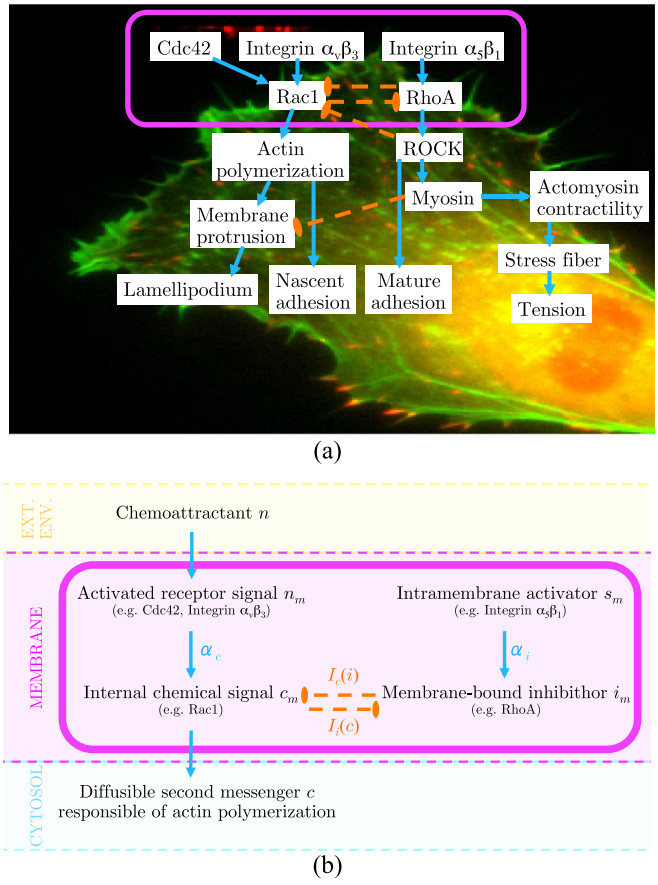


FIG. 10. Examples of intracellular pathways regulating actin polymerization and cell motion: (a) detailed representation of the biological cascade of intracellular proteins and molecules involved in the whole process (modified with permission from Ref. [81]); (b) simplified network of reaction considered to derive the relation between the external chemical field $n$ and the polymerizing factor $c$, through reactions occurring at the cell membrane only. The cyan solid arrows represent positive activation, whereas the orange dashed lines stands for negative down-regulations. The abbreviation "Ext. Env." stands for external environment.

introductory section, the cell chemotactic response is mediated through the binding of the detected external signal to certain classes of surface receptors and through its subsequent transduction to internal pathways. Therefore in the second scenario, we consider a more complex link between the perception of the chemoattractant and the polymerizing factor at the cell membrane. To be specific, we here postulate a mutually inhibitory feedback loop between the polymerizing factor at the cell membrane $c_m$ and its intramembrane inhibitor, $i_m$, regulated by the membrane activator, $s_m$ [see Fig. 10(b)]. This can be, for instance, related to the Rac1-RhoA dynamics [83,84] [see Fig. 10(a)], whose concentrations take respectively the role of the intracellular signaling molecule at the cell membrane $c_m$ and its inhibitor $i_m$. For sake of simplicity, as done, for instance, in Ref. [85], we neglect the details of the binding process of the chemoattractant to the receptors, and we assume that the signal $n_m$ generated by the integrin $\alpha_v\beta_3$ engagement and by Cdc42, which stimulates Rac1 at the membrane, is directly related to the external chemoattractant concentration $n$, so that the simplified subcellular network can be represented by Fig. 10(b). With this choice we do not claim to be exhaustive and we are aware that a huge literature of polarity and chemotaxis models exists (see, for instance, the review works [53,82,86–88] and the Rho GTPases models [89–91]). However, so far, no model or set of models have been proven to be able to capture all the features possibly occurring in moving eukatyotic cells (see Refs. [53,86,87] for advantages and drawbacks of each class of models). Typically, polarization is modeled by reaction diffusion systems, explaining symmetry breaking from the front to the back of the cell, and two approaches are used: the first is to consider the diffusion of chemicals inside the whole cell or a portion of it, with appropriate inhibitory mechanisms to cluster the signal at the membrane [53,55,92], alternatively, some models describe chemical distributions only along the cell perimeter, with eventually some second messengers diffusing inside the cytosol [85,86]. In the present work we follow the second route, in order to maintain a single fast-diffusing chemical regulating actin polymerization inside the cell, as a result of complex biochemical pathways occurring at the cell membrane. This modeling approach is consistent with

the biological observation that the Rho GTPases (e.g., Cdc42, RhoA, and, at least in some cells, Rac) in their active forms have been found predominantly bound to membranes and not cytosolic [93,94]. Therefore, the process of conversion of the external stimulus into an intracellular second messenger is likely to occur at (or possibly, close to) the cell membrane. Then, we decided to focus on the Rho GTPase dynamics, since these molecules play a central role in all eukaryotic cells, controlling the organization of the actin cytoskeleton and adhesion [94] and have been less studied than the well-known PI3K pathway [92,95]. As suggested by the biological findings in Ref. [84], we exploit a negative feedback loop as a transduction mechanism at the cell membrane, since, in principle, signal amplification does not need to involve a positive feedback [53], as postulated in previous works [90,91]. The biochemical model underlying the mutually inhibitory feedback loop, without considering the diffusion of the chemical inside the membrane, which is very slow [93], taking all concentrations dimensionless for sake of simplicity, is given by the following set of equations [96]:

$$\begin{cases} \dfrac{\partial c_m}{\partial t} = \alpha_c(n_m - c_m) - I_c(i_m)c_m \\ \dfrac{\partial i_m}{\partial t} = \alpha_i(s_m - i_m) - I_i(c_m)i_m \end{cases} \quad \text{for } m = \{a, b\}, \tag{18}$$

where $\alpha_c$ and $\alpha_i$ are the rates of synthesis and degradation of the chemical factors $c_m$ and $i_m$, respectively, and $I_c$ and $I_i$ stand for the feedback inhibition of $c_m$ and $i_m$, that can be modeled by Hill kinetics [97], so that

$$I_c(i_m) = \frac{\beta_c i_m^d}{K_c^d + i_m^d}, \quad I_i(c_m) = \frac{\beta_i c_m^d}{K_i^d + c_m^d}. \tag{19}$$

Biologically, $K_{\{c,i\}}$ represents the ligand concentration producing half occupation of the binding sites of the repressed target, whereas the Hill coefficient $d$ modulates the degree of function sigmoidity and identifies the level of nonlinearity exhibited by the feedback loop. We remark that the biochemical feedback loop, defined by Eq. (18), is assumed to hold only at the cell membrane [i.e., in $x = \{a, b\}$], and it is responsible of determining the boundary condition, $c_a$ and $c_b$, for the polymerizing signal $c$ diffusing inside the cytosol, accordingly to Eq. (9).

Then, considering the stationary conditions for the system (18), it is possible to obtain the relation linking the external chemical field at the cell boundaries $n_m$ to the concentration of the polymerizing factor at the membrane:

$$n_m = \left[1 + \frac{1}{\alpha_c} I_c\left(\frac{\alpha_i s_m}{\alpha_i + I_i(c_m)}\right)\right] c_m \text{ for } m = \{a, b\}. \tag{20}$$

The relation (20) between the polymerizing factor and the value of the external chemotactic field at the cell boundary is plotted in Fig. 9(b), (top). In this case, the resulting relation between the cell velocity and the chemoattractant gradient, obtained by means of Eq. (20), is far more complex and is represented by a bistable curve [Fig. 9(b), bottom] characterized by the presence of what we will call in the following a lower turning point (for lower values of $c_m$ and higher values of $n_m$) and a higher turning point (for higher values of $c_m$ and lower values of $n_m$). In particular, for chemical concentration gradients between the two cells ends below a threshold [red square diamond in Fig. 9(b), bottom], the cell is not able to respond to the external chemical cue. This critical value stands for the slightest difference in the external chemical field at cells ends that is able to induce the polarization of the cell and it is related to the internal threshold set for the polymerization of the actin network. We remark that this threshold is in agreement with the biological observation that the cell cannot detect too shallow chemical gradients [77,98]. Above this critical value for the normalized chemoattractant gradient, the cell crawls with a velocity which is almost linearly growing with increasing gradients of the chemoattractant field, until the external gradient is so steep that the cell switches [green (light gray) pointed arrow in the lower figure in Fig. 9(b), corresponding to the lower turning point in the upper figure] to the upper branch of the curve, characterized by higher velocities that grows up to a saturation level [see the green (light gray) curve in Fig. 9(b), bottom]. We remark that the green (light gray) curve in Fig. 9(b) (bottom) qualitatively reproduces the ones reported in Song *et al.* [98] using *Dictyostelium discoideum* cells migrating inside a linear gradients of cyclic adenosine monophosphate (cAMP), at least in a certain range of chemical gradients. Indeed, the experimental work in [98] demonstrates the existence of a lower threshold in the chemical gradient [which corresponds to the red square diamond in Fig. 9(b) (bottom), below which the cell experiences random motion, but the velocity components took average values close to zero; above this threshold, cells exhibit a directional response and the chemotactic speed increases gradually with increasing steepness of the gradient until, for a given chemotactic gradient [corresponding to the green (light gray) pointed arrow in the lower figure in Fig. 9(b)], the velocity abruptly increases up to its maximum value. Then the same experimental work [98] reports a decrease in the cell migratory ability in response to increasing chemical gradient, which cannot be reproduced by our curves since it is likely related to the existence of a second threshold in polymerization [98], not included in our model. Conversely, decreasing the external chemical gradient, the velocity of the migrating cell decreases following the blue (dark gray) curve in Fig. 9(b) (bottom): the cell persistently migrates with higher velocities inside the external chemical field with a less steep gradient, until the external gradient is so shallow that the cell velocity rapidly decreases [blue (dark gray) pointed arrow in the lower figure in Fig. 9(b), corresponding to the upper turning point in the upper figure], and then, for even smaller gradients, the cell stops. We remark that the values of external chemical concentration gradient corresponding to the two arrows above define an interval in which a double-well potential exists, and the temporal evolution of the perception of the chemoattractant (possibly influenced by the presence of noise [99]) will set on which branch the cell will be. This interval of coexistence enlarges if, for instance, the upper turning point corresponding to the blue (dark gray) arrow moves to the left. In the limit in which the upper turning point is formally assumed for negative values, the upper branch in the graphs in Fig. 9(a) always exists, as shown in differentiation processes described in Ref. [100]. In this case, after reaching the upper branch, the cell can persist in its motion even if the chemotactic cue is switched off.

This bistable behavior cannot be confirmed by the experimental works by Song *et al.* [98], since cell migration onto decreasing values of chemoattractant field was not studied in that work. However, the capability of cells to exhibit long-term memory have been experimentally observed [82,101], leading to speculations on the existence of bistable switchlike memory modules.

In principle the same reasoning used in this section for the chemotactic field can be applied to mechanically induced polarization and motion as that shown in Ref. [74]. Indeed, it is known that the adhesion with the substrate can activate various signal-transduction pathways that regulate actin polymerization and depolymerization, through the expression of different internal chemical signals. However, we remark that, in the case of mechanically induced polymerization, the effect of external loads and internal stresses on the active stress, $\chi$, and on the frictional parameter, $\beta$, cannot be neglected.

## IV. CONCLUSIONS

In this work we have illustrated a continuous mechanical model for describing cell chemotaxis on a two-dimensional flat and rigid substrate, considering the subcellular actin dynamics. The whole polymerization-depolymerization process is controlled by an intracellular polymerizing factor, which acts as a second messenger during cell chemotaxis in response to the external chemical field.

The proposed model, bridging the gap between the mechanical models of cell migration [11,33–39] and the models describing cell chemotaxis [49–55], represents an advancement with respect to the state of the art. Indeed, we take into account not only the mechanical effect involved in cell chemotaxis, such as the mechanical interaction with the substrate, the passive (viscous) and active properties of the cell (described as a gel composed by the actin network immersed in the cytosolic liquid), but also the dynamics of actin assembly and disassembly guided by intracellular chemical cues. Differently from previous works combining the cell mechanics with chemical cues [59,59–61], we have kept the model as simple as possible in order to investigate possible relations between the cell velocity and the external chemical field. At the same time, our approach substantially differs from the work of Yang *et al.* [62], in which a quantitative relationship between cell motility and chemotactic gradient has been derived, considering the different physical forces acting on the cell, treated as a rigid body and neglecting the cell mechanical behavior.

The model equations have been numerically discretized and solved in order to obtain the distribution in time and space inside the cell of the stress, the polymerizing factor, the actin monomers, and the lamellipodium branched actin filaments. In agreement with biological experiments, we observe that the lamellipodial actin abruptly disappears about few $\mu$m beyond the leading edge [17], while the actin monomers form a widespread pool inside the cell available for the formation of different types of actin [16]. The numerical results also predict the formation of a steep intracellular signaling molecule gradient that amplifies external shallow chemoattractant variations. Furthermore, we show that the polymerizing factor can be linked, for instance, to the external chemoattractant availability, and we analyze the cell traveling velocity with respect to the external chemical gradient, considering different mechanisms of activation of the intracellular second messenger. The possibility to include *a posteriori* in the model the relation between the internal signaling molecules and the external chemical field is a point of strength of the proposed model, since it allows us to easily test different mechanisms of chemical signal transmission and conversion inside the cell and to possibly include the dependency from other external factors inside the model (e.g., mechanical stresses during mechanically induced polarization and motion). In this respect, the proposed model is able to reproduce the absence of directed migration of a cell inside too shallow chemical gradients, when no spontaneous polarization occurs, and the different mechanisms of migration in response to various gradients and intensities of chemoattractant field.

Without claiming to provide quantitative numerical measurements, the results presented in this work can be evaluated as a proof of concept towards the definition of a comprehensive model of cell chemotaxis, taking into account cell mechanics and internal chemical kinetics. Nonetheless, these results need to be quantitatively validated by comparing the predicted evolution with the real spatiotemporal evolution of the different quantities inside the moving cell.

Finally, in constructing the model, we have made some simplifications, that deserve to be studied in more details, such as the role of mechanical stresses on the actin polymerization and depolymerization process, the mutual interaction between chemical and mechanical cues and the refinement of the description of the subcellular pathways converting the chemical and mechanical external cues in the internal signaling regulating the whole process. In particular, it could be interesting to investigate the role of mechanical stresses and myosin contractility during the transient polarization process (i.e., when the cell passes from the state at rest to the motile one) and during the whole cell migration. The introduction of a dependence of the polymerization velocity on a mechanical load [37], as well as the dependence of the stress field on the myosin concentration would be straightforward [35], in spite of requiring the introduction of an equation describing the nonhomogeneous distribution of myosin motors and their coupling with actin dynamics. Future investigations will be certainly devoted to a more detailed description of the cell-substrate adhesion and of the mechanotransduction process, with the inclusion of mechanical feedbacks within the model itself. Regarding the biochemical aspects of the proposed model, future works should address the introduction of more complex mechanisms of signal conversion at the cell membrane, in order to account for cell adaptation [82], i.e., the capability to respond to the gradient itself rather than to the absolute value of the signal [86]. Specifically, the capability of the system to adapt to external gradient can be added in our model, by including either a specific module for adaptation or two complementary signals: a fast, local activation signal followed by a slower, global inhibition signal, both of which are regulated by the external stimulus, such as in the well-known LEGI model [82]. Therefore future works will couple different receptor-mediated signaling pathways implicated in gradient sensing at the cell membrane, along with multiple cytosolic chemical factors acting on the different stages of polarization. Finally, it is desirable, from the biological

point of view, to have a more comprehensive understanding of the multiple control mechanisms, by identifying specific molecules and their influence on cell motility [82]. Indeed, the elucidation of the biochemical pathways underlying cell motion in response to different external and internal factors will have a significant impact on understanding physiological cell behavior as well as human diseases such as cancer and inflammation.


## ACKNOWLEDGMENT

The authors wish to thank the Istituto Nazionale di Alta Matematica "F. Severi" for partial funding of this work.



[1] D. Bray, *Cell Movements: From Molecules to Motility* (Garland Science, New York, 2000).

[2] B. Alberts, A. Johnson, J. Lewis, M. Raff, K. Roberts, and P. Walter, *Molecular Biology of the Cell* (Garland Science, New York, 2002).

[3] M. Abercrombie, J. E. Heaysman, and S. M. Pegrum, Exp. Cell Res. **59**, 393 (1970).

[4] T. Stossel, Science **260**, 1086 (1993).

[5] A. Mogilner and L. Edelstein-Keshet, Biophys. J. **83**, 1237 (2002).

[6] A. V. Vorotnikov, Biochemistry (Mosc.) **76**, 1528 (2011).

[7] A. Ridley, M. Schwartz, K. Burridge, R. Firtel, M. Ginsberg, G. Borisy, J. Parsons, and A. Horwitz, Science **302**, 1704 (2003).

[8] E. Barnhart, K. Lee, K. Keren, A. Mogilner, and J. Theriot, PLoS Biol. **9**, e1001059 (2011).

[9] G. Danuser, J. Allard, and A. Mogilner, Annu. Rev. Cell Dev. Biol. **29**, 501 (2013).

[10] R. Ananthakrishnan and A. Ehrlicher, Int. J. Biol. Sci. **3**, 303 (2007).

[11] B. Rubinstein, M. Fournier, K. Jacobson, A. B. Verkhovsky, and A. Mogilner, Biophys. J. **97**, 1853 (2009).

[12] K. Kruse, J. Joanny, F. Julicher, and J. Prost, Phys. Biol. **3**, 130 (2006).

[13] C. Wilson, M. Tsuchida, G. Allen, E. Barnhart, K. Applegate, P. Yam, L. Ji, K. Keren, G. Danuser, and J. Theriot, Nature (London) **465**, 373 (2010).

[14] P. Vallotton, G. Danuser, S. Bohnet, J.-J. Meister, and A. B. Verkhovsky, Mol. Biol. Cell **16**, 1223 (2005).

[15] T. M. Svitkina, A. B. Verkhovsky, K. M. McQuade, and G. G. Borisy, J. Cell Biol. **139**, 397 (1997).

[16] E. S. Chhabra and H. N. Higgs, Nat. Cell Biol. **9**, 1110 (2007).

[17] A. Ponti, M. Machacek, S. Gupton, C. Waterman-Storer, and G. Danuser, Science **305**, 1782 (2004).

[18] X. Jiang, D. A. Bruzewicz, A. P. Wong, M. Piel, and G. M. Whitesides, Proc. Natl. Acad. Sci. U.S.A. **102**, 975 (2005).

[19] A. V. Vorotnikov and P. A. Tyurin-Kuzmin, Genes Dis. **1**, 162 (2014).

[20] I. S. Aronson, *Physical Models of Cell Motility* (Springer International, 2016).

[21] F. Ziebert, S. Swaminathan, and I. Aranson, J. R. Soc. Interface **9**, 1084 (2012).

[22] L. Li, S. F. Nørrelykke, and E. C. Cox, PLoS ONE **3**, e2093 (2008).

[23] K. F. Swaney, C.-H. Huang, and P. N. Devreotes, Annu. Rev. Biophys. **39**, 265 (2010).

[24] Y. Sakumura, Y. Tsukada, N. Yamamoto, and S. Ishii, Biophys. J. **89**, 812 (2005).

[25] Y. Wang, H. Senoo, H. Sesaki, and M. Iijima, Proc. Natl. Acad. Sci. U.S.A. **110**, E4723 (2013).

[26] G. Servant, O. Weiner, P. Herzmark, J. W. Balla, T. Sedat, and H. R. Bourne, Science **287**, 1037 (2000).

[27] C. Janetopoulos, L. Ma, P. Devreotes, and P. Iglesias, Proc. Natl. Acad. Sci. U.S.A. **101**, 8951 (2004).

[28] A. Samadani, J. Mettetal, and A. van Oudenaarden, Proc. Natl. Acad. Sci. U.S.A. **103**, 11549 (2006).

[29] P. Recho, T. Putelat, and L. Truskinovsky, J. Mech. Phys. Solids **84**, 469 (2015).

[30] A. Mogilner, J. Math. Biol. **58**, 105 (2009).

[31] H. Yamaoka, S. Matsushita, Y. Shimada, and T. Adachi, Biomech. Model Mechanobiol. **11**, 291 (2012).

[32] L. S. Kimpton, J. P. Whiteley, S. L. Waters, and J. M. Oliver, J. Math. Biol. **70**, 133 (2015).

[33] W. Alt and R. Tranquillo, J. Biol. Syst. **3**, 905 (1995).

[34] D. Shao, H. Levine, and W. Rappel, Proc. Natl. Acad. Sci. U.S.A. **109**, 6851 (2012).

[35] P. Recho and L. Truskinovsky, Phys. Rev. E **87**, 022720 (2013).

[36] P. Recho, T. Putelat, and L. Truskinovsky, Phys. Rev. Lett. **111**, 108102 (2013).

[37] D. Ambrosi and A. Zanzottera, Phys. D **330**, 58 (2016).

[38] M. Gracheva and H. Othmer, Bull. Math. Biol. **66**, 167 (2004).

[39] K. Larripa and A. Mogilner, Physica A **372**, 113 (2006).

[40] K. Kruse, J. Joanny, F. Jülicher, J. Prost, and K. Sekimoto, Eur. Phys. J. E **16**, 5 (2005).

[41] F. Julicher, K. Kruse, J. Prost, and J. Joanny, Phys. Rep. **449**, 3 (2007).

[42] J. Joanny, F. Julicher, K. Kruse, and J. Prost, New J. Phys. **9**, 422 (2007).

[43] K. Doubrovinski and K. Kruse, Phys. Rev. Lett. **107**, 258103 (2011).

[44] M. Dembo and F. Harlow, Biophys. J. **50**, 109 (1986).

[45] W. Alt and M. Dembo, Math. Biosci. **156**, 207 (1999).

[46] M. Herant, W. A. Marganski, and M. Dembo, Biophys. J. **84**, 3389 (2003).

[47] L. S. Kimpton, J. P. Whiteley, S. L. Waters, J. King, and J. M. Oliver, Math. Med. Biol. **30**, 241 (2013).

[48] Y. Mori, A. Jilkine, and L. Edelstein-Keshet, Biophys. J. **94**, 3684 (2008).

[49] T. Hillen and K. J. Painter, J. Math. Biol. **58**, 183 (2009).

[50] E. Keller and L. Segel, J. Theor. Biol. **30**, 225 (1971).

[51] J. Haugh and D. Lauffenburger, Biophys. J. **72**, 2014 (1997).

[52] M. Iijima, Y. Huang, and P. Devreotes, Dev. Cell **3**, 469 (2002).

[53] A. Levchenko and P. A. Iglesias, Biophys. J. **82**, 50 (2002).

[54] H. Meinhardt and A. Gierer, BioEssays **22**, 753 (2000).

[55] C. Parent and P. Devreotes, Science **284**, 765 (1999).

[56] A. Marée, V. Grieneisen, and L. Edelstein-Keshet, PLoS Comput. Biol. **8**, e1002402 (2012).

[57] M. Neilson, D. Veltman, P. van Haastert, S. Webb, J. Mackenzie, and R. Insall, PLoS Biol. **9**, e1000618 (2011).

[58] G. MacDonald, J. Mackenzie, M. Nolan, and R. Insall, J. Comput. Phys. **309**, 207 (2016).
[59] C. Elliott, B. Stinner, and C. Venkataraman, J. R. Soc. Interface **9**, 3027 (2012).
[60] C. Shi, C.-H. Huang, P. Devreotes, and P. Iglesias, PLoS Comput. Biol. **9**, e1003122 (2013).
[61] A. Moure and H. Gomez, Biomec. Model. Mechanobiol. **17**, 1243 (2018).
[62] H. Yang, X. Gou, Y. Wang, A.-H. Fahmy, T. M. Leung, J. Lu, and S. Sun, Biophys. J. **108**, 1645 (2015).
[63] J. Howard, S. W. Grill, and J. S. Bois, Nat. Rev. Mol. Cell Biol. **12**, 392 (2011).
[64] T. Kole, Y. Tseng, I. Jiang, J. Katz, and D. Wirtz, Mol. Biol. Cell **16**, 328 (2005).
[65] P. Pullarkat, P. Fernandez, and A. Ott, Phys. Rep. **449**, 2953 (2007).
[66] A. Mogilner and G. Oster, Biophys. J. **71**, 3030 (1996).
[67] G. E. Jones, W. E. Allen, and A. Ridley, Cell Adhes. Commun. **6**, 237 (1998).
[68] M. Fournier, R. Sauser, D. Ambrosi, J. Meister, and A. Verkhovsky, J. Cell Biol. **188**, 287 (2010).
[69] M. Postma, L. Bosgraaf, and H. Loovers, EMBO Rep. **5**, 35 (2004).
[70] C. A. Reinhart-King, M. Dembo, and D. A. Hammer, Biophys. J. **89**, 676 (2005).
[71] J.-P. Rieu, C. Barentin, Y. Maeda, and Y. Sawada, Biophys. J. **89**, 3563 (2005).
[72] A. Diz-Muñoz, D. Fletcher, and O. Weiner, Trends Cell Biol. **23**, 47 (2013).
[73] L. Picas, F. Rico, and S. Scheuring, Biophys. J. **102**, L01 (2012).
[74] A. B. Verkhovsky, T. M. Svitkina, and G. Borisy, Curr. Biol. **9**, 11 (1999).
[75] T. D. Pollard, L. Blanchoin, and R. D. Mullins, Annu. Rev. Biophys. Biomol. Struct. **29**, 545 (2000).
[76] M. Postma and P. J. M. Van Haastert, Biophys. J. **81**, 1314 (2001).
[77] A. T. Sasaki and R. A. Firtel, Eur. J. Cell Biol. **85**, 873 (2006).
[78] S. Gupton and C. Waterman-Storer, Cell **125**, 1361 (2006).
[79] S. Palecek, J. Loftus, M. Ginsberg, D. Lauffenburger, and A. Horwitz, Nature (London) **385**, 537 (1997).
[80] A. Huttenlocher, M. H. Ginsberg, and A. F. Horwitz, J. Cell. Biol. **134**, 1551 (1996).
[81] J. Small, B. Geiger, I. Kaverina, and A. Bershadsky, Nat. Rev. Mol. Cell. Biol. **3**, 957 (2002).
[82] P. A. Iglesias and A. Levchenko, Sci. STKE **2002**, re12 (2002).
[83] F. Van Leeuwen, H. Kain, R. Van Der Kammen, F. Michiels, O. Kranenburg, and J. Collard, J. Cell Biol. **139**, 797 (1997).
[84] K. M. Byrne, N. Monsefi, J. C. Dawson, A. Degasperi, J.-C. Bukowski-Wills, N. Volinsky, M. Dobrzyński, M. R. Birtwistle, M. A. Tsyganov, A. Kiyatkin, K. Kida, A. J. Finch, N. O. Carragher, W. Kolch, L. K. Nguyen, A. von Kriegsheim, and B. N. Kholodenko, Cell Syst. **2**, 38 (2016).
[85] H. Levine, D. A. Kessler, and W.-J. Rappel, Proc. Natl. Acad. Sci. U.S.A. **103**, 9761 (2006).
[86] A. Jilkine and L. Edelstein-Keshet, PLoS Comput. Biol. **7**, e1001121 (2011).
[87] P. Devreotes and C. Janetopoulos, J. Biol. Chem. **278**, 20445 (2003).
[88] P. A. Iglesias and P. N. Devreotes, Curr. Opin. Cell Biol. **20**, 35 (2008).
[89] M. Otsuji, S. Ishihara, C. Co, K. Kaibuchi, A. Mochizuki, and S. Kuroda, PLoS Comp. Biol. **3**, e108 (2007).
[90] A. Jilkine, A. Marée, and L. Edelstein-Keshet, Bull. Math. Biol. **69**, 1943 (2007).
[91] C. M. Simon, E. M. Vaughan, W. M. Bement, and L. Edelstein-Kesheta, Mol. Biol. Cell. **24**, 421 (2013).
[92] A. Gamba, A. de Candia, S. Di Talia, A. Coniglio, F. Bussolino, and G. Serini, Proc. Natl. Acad. Sci. U.S.A. **102**, 16927 (2005).
[93] K. Kaibuchi, S. Kuroda, and M. Amano, Annu. Rev. Biochem. **68**, 459 (1999).
[94] D. J. G. Mackay and A. Hall, J. Biol. Chem. **273**, 20685 (1998).
[95] A. Narang, K. Subramanian, and D. Lauffenburger, Ann. Biomed. Eng. **29**, 677 (2001).
[96] J. S. Griffith, J. Theor. Biol. **20**, 202 (1968).
[97] U. Alon, *An Introduction to Systems Biology: Design Principles of Biological Circuits*, CRC Mathematical and Computational Biology (Chapman and Hall/CRC, 2007), Vol. 10.
[98] L. Song, S. Nadkarni, H. Bödeker, C. Beta, A. Bae, C. Franck, W.-J. Rappel, W. Loomis, and E. Bodenschatz, Eur. J. Cell Biol. **85**, 981 (2006).
[99] V. te Boekhorst, L. Preziosi, and P. Friedl, Ann. Rev. Cell Dev. Biol. **32**, 491 (2016).
[100] W. Xiong and J. Ferrell, Nature (London) **426**, 460 (2003).
[101] M. Skoge, H. Yue, M. Erickstad, A. Bae, H. Levine, A. Groisman, W. F. Loomis, and W.-J. Rappel, Proc. Natl. Acad. Sci. U.S.A. **111**, 14448 (2014).